



Assessing the potential for an ice core in the southern Antarctic Peninsula to elucidate Holocene climate history

Harry J. Davis¹, Robert G. Bingham¹, Carlos Martín², Elizabeth R. Thomas², Andrew S. Hein¹, and Anna E. Hogg³

Correspondence: Harry J. Davis (h.davis@ed.ac.uk)

Abstract. Connecting the West Antarctic Ice Sheet to the southern Antarctic Peninsula, northern Ellsworth Land is a region of enigmatic glacial history now experiencing significant cryospheric change. Large portions of the Bellingshausen-Sea-draining basins have experienced extreme ice thinning and grounding-line change over the satellite observation period. However, the Holocene glacial history of northern Ellsworth Land, which would help to frame the contemporary changes being observed, is poorly constrained. High-resolution ice cores are crucial for reconstructing this past ice-sheet change. We identify a new deep ice-core drilling site at the triple-ice divide point between the Amundsen, Bellingshausen, and Weddell seas (74°34'37" S, 86°54'16" W) that could be utilised to address this knowledge gap. Using a transient ice-thinning model, constrained by shallow-ice-core data and dated englacial radar stratigraphy, we estimate records of accumulation and derive a preliminary age-depth scale for the proposed coring site. Inclusion of dated radar stratigraphy in the model improves our constraints on the long-term climate history, and highlights that these data are not compatible with a steady-state assumption. We also show that there has been a significant change in the accumulation rate regime or ice thickness throughout the Holocene. A deep ice core at this site would provide a climate record up to \sim 30 ka with a resolution of 0.58 ka/m at 60 m above the ice-bed interface. An analysis of the model sensitivity to basal melting shows that a record beyond the onset of the Holocene could still be recovered under high basal-melt-rate scenarios. We thus conclude that an ice core at this site would yield a valuable high-resolution climate record and provide precise constraints to reconstruct climatic changes and glacial retreat during the Holocene, to help resolve the onset of the extensive dynamic thinning observed today.

1 Introduction

The West Antarctic Ice Sheet (WAIS) is hypothesised to be vulnerable to major collapse with climate warming (Mercer, 1978) and has the potential to contribute several metres to global sea level rise (Edwards et al., 2021; Pritchard et al., 2025). With much of the WAIS grounded in marine basins up to 2,000 m below sea level (Lythe and Vaughan, 2001; Fretwell et al., 2013; Morlighem et al., 2017; Pritchard et al., 2025), the area is highly susceptible to mass loss as a result of marine-ice-sheet instability (MISI) induced by ocean warming (Weertman, 1974; Mercer, 1978; Thomas and Bentley, 1978; Pattyn and Morlighem, 2020). Dynamic thinning observed around the ice-sheet margins (Pritchard et al., 2009; Shepherd et al., 2019) has

¹School of GeoSciences, University of Edinburgh, Edinburgh, UK

²British Antarctic Survey, Cambridge, UK

³School of Earth and Environment, University of Leeds, Leeds, UK





gradually progressed inland (Otosaka et al., 2023), and has motivated scientific research programmes to investigate whether MISI is underway (Alley et al., 2015; Scambos et al., 2017). The vulnerability of ice to MISI in northern Ellsworth Land, where the WAIS meets the Antarctic Peninsula Ice Sheet (APIS) (Figure 1), remains poorly constrained and is the focus of this study.

Satellite observations of northern Ellsworth Land have highlighted significant modern ice losses (Wouters et al., 2015; Christie et al., 2016), acceleration (Gardner et al., 2018), and thinning (Shepherd et al., 2019; Nilsson et al., 2022) along the Bellingshausen Sea coastline in recent decades, analogous to the processes observed in the Amundsen Sea Embayment (Turner et al., 2017). Larter et al. (2014) note that current thinning rates are elevated compared to those interpreted from palaeoglacial records (Bentley et al., 2014) but it is unclear whether these contemporary changes are unprecedented during the Holocene due to the large gaps in available data (Jones et al., 2022). Therefore, there is a need to improve our understanding of the vulnerability of ice across northern Ellsworth Land in the face of continued climate warming.

One way to understand better contemporary thinning trends in the context of longer-term change is through ice core analysis (Raynaud and Lebel, 1979). The chemical composition of an ice core can reveal information about the climatic conditions during snowfall deposition (Thomas et al., 2017). Subsequent dating of the ice core through annual layer counting (Sigl et al., 2016; Hoffmann et al., 2022; Emanuelsson et al., 2022), correlation with dated volcanic eruptions (Narcisi et al., 2006; Fujita et al., 2015), comparison of chemical species with other ice cores (Monnin et al., 2004), or ice-flow modelling (?Martín et al., 2015; Rowell et al., 2023), can be used to establish an ice-core chronology. These climate records can extend from a few hundred years to thousands of years, and further analyses of the chemical composition of ice layers can give insights into ice-thinning patterns (Raynaud and Lebel, 1979; Grieman et al., 2024), and provide precise constraints for ice-sheet models to reconstruct past ice-sheet configurations (Sutter et al., 2021; Wolff et al., 2025) and infer palaeo-accumulation rates (Martín et al., 2015).

In this paper, we explore the potential for ice at the triple-divide of Pine Island Glacier, Ferrigno Ice Stream and Evans Ice Stream (74°34'37" S, 86°54'16" W; Figure 1) to yield a deep ice core of high resolution suitable for reconstructing Holocene ice and climate history where the WAIS merges with the APIS. As the site also represents the divide between ice draining to the Amundsen, Bellingshausen and Weddell seas, hereafter for convenience we term the proposed ice core location ABW. We first introduce the ABW site, then provide an overview of the radio-echo sounding (RES) and shallow ice-core data that we use to constrain our modelling. We then describe the one-dimensional (1-D) ice-flow model (Martín et al., 2015; Rowell et al., 2023), and our approach to constraining the model with age observations, to produce a reconstruction of past accumulation rates throughout the Holocene and into the Last Glacial Period (LGP).

2 Datasets and Methods

2.1 Site Characteristics

The ABW site is situated in northern Ellsworth Land at the intersection of the Amundsen, Bellingshausen, and Weddell ice divides (74°34'37" S, 86°54'16" W), where ice is 1,220 m deep (Bingham et al., 2012) and ice-surface elevation is 1,350 m





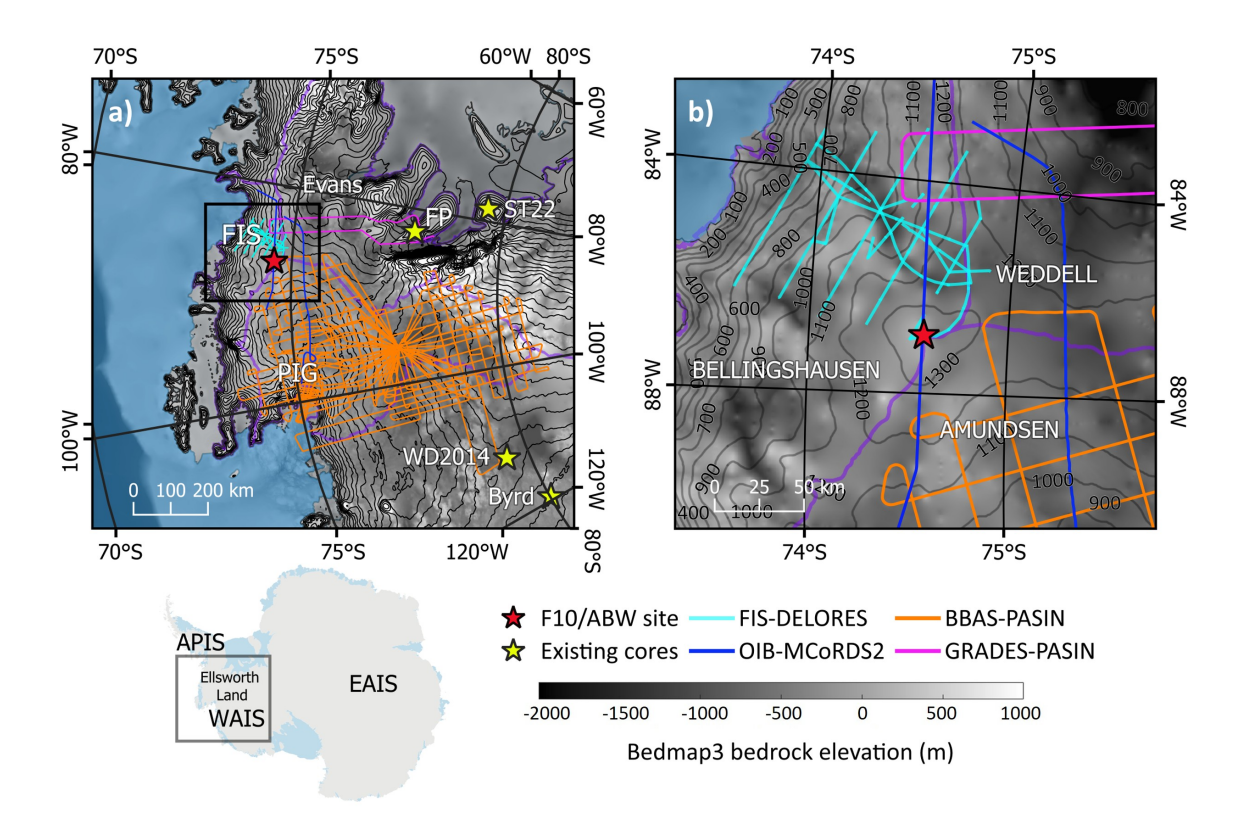


Figure 1. Maps of study area with the datasets and key locations mentioned in this study. (a) Zoom in to northern Ellsworth Land. (b) Zoom in to specific study region. FIS and Evans refer to Ferrigno and Evans Ice Streams, respectively, while PIG refers to Pine Island Glacier. Byrd, WD2014 (WAIS Divide), FP (Fletcher Promontory), and ST22 (Skytrain Ice Rise) denote previous deep ice-core drilling sites. The ice divides of the Bellingshausen, Amundsen, and Weddell Sea drainage basins are shown in purple (Zwally et al., 2012), with bedrock elevation data from Pritchard et al. (2025), and CryoSat-2 100 m surface-elevation contours from Helm et al. (2014). Orange, dark blue, light blue and magenta profiles in (a) and (b) show RES profiles, details for which are outlined in Section 2.2.1 and Table 1. The inset below (a) locates the study area. Maps are generated using the Quantarctica mapping environment in QGIS (Matsuoka et al., 2021).

(Helm et al., 2014) (Figure 1). The site sits astride a topographic high along the triple-ice-divide on otherwise relatively flat bedrock. Ice flow diverges in three directions away from the divide at a speed of less than 10 m/yr (Slater et al., In Prep). Shallow ice core data show that surface accumulation rates increased by 27 % between 2000 and 2010 from a previously stable annual average snow accumulation of 33 cm/yr before 1900 (Thomas et al., 2015). An automatic weather station was located at the site from December 2009 to December 2010 and showed the monthly average 2 m temperature to range from $-15^{\circ}C$ in summer to $-30^{\circ}C$ in winter and the annual average wind speed to be around 9.4 m/s (Thomas and Bracegirdle, 2014).





Table 1. Summary of the three RES systems used in this study.

System	Year	Platform	Centre Frequency	Bandwidth/ pulse width	Vertical Resolution	References
DELORES	2009/10	Ground-based	3 MHz	10 MHz	11.1 m	(King, 2020)
PASIN	2004-2007	Twin Otter	150 MHz	10 MHz/ 100 ns	12.89/ 8.42 m	(Vaughan et al., 2006)
MCoRDS2	2018	DC8	190 MHz	50 MHz	2.58 m	(Rodriguez-Morales et al.,
						2014; Arnold et al., 2020)

Note: For the PASIN system, we use data from both the chirp- and pulse-acquisition modes and list their individual characteristics in the bandwidth and vertical resolution columns. The vertical resolution for the MCoRDS2 is calculated as per CReSIS (2024) using a scaling factor "k" - see Bodart et al. (2021) for more details.

2.2 Radiostratigraphy

2.2.1 Radio-echo sounding datasets

We use a combination of airborne and ground-based RES data from several field campaigns throughout West Antarctica between 2004 and 2018. The main surveys include two British Antarctic Survey (BAS) field campaigns that used the Polarimetric Airborne Survey INstrument (PASIN), (1) the 2004/05 BBAS survey over Pine Island Glacier (Vaughan et al., 2006) (hereafter termed "PIG-PASIN"), and (2) the 2006/07 GRADES-IMAGE survey of Evans and Rutford ice streams (Ashmore et al., 2014; Corr, 2021) (hereafter termed "GRADES-PASIN"); an extensive ground-based survey of Ferrigno Ice Stream in 2009/10 (Bingham et al., 2012) using the ground-based BAS DEep-LOoking Radio-Echo Sounder (DELORES; King (2020)); and two profiles from NASA's Operation IceBridge (OIB; MacGregor et al. (2021)) surveys in 2016 and 2018 using the Multichannel Coherent Radar Depth Sounder 2 (MCoRDS2; CReSIS (2024)). Table 1 summarises the relevant information for each RES system. Crucially, each of the RES systems has imaged multiple internal-reflection horizons (IRHs) which act as isochrones across the WAIS (Siegert, 1999). We note that although these RES data were acquired over a period spanning 14 years, modern snow accumulation has been insufficient to induce vertical lowering of internal layers beyond the vertical resolution of each RES system and hence the radiostratigraphies derived from each RES dataset can be considered contemporaneous.

2.2.2 Tracing internal-reflection horizons (IRHs)

It is now well established that IRHs in Antarctic RES data largely arise from variations in electrical conductivity related to palaeo-accumulation events, and can thus be treated as isochrones (Bingham et al., 2025). We traced IRHs through the RES data using Schlumberger Petrel® 3-D seismic software, applying a semi-automated layer picking algorithm that tracks the local maxima of the received reflections between individual traces. We initiated IRH tracing in the Pine Island Glacier catchment (A in Figure 2 and Figure A1), where Bodart et al. (2021) had previously traced three IRHs aged, 2.62 ± 0.31 ka, 4.72 ± 0.28 ka and 6.94 ± 0.31 ka through the PIG-PASIN dataset. Hereafter we will abbreviate these ages as 2.62, 4.72 and 6.94 ka. Even though the OIB-MCoRDS2 system characteristics differ with the PASIN system (Table 1), these three prominent time markers





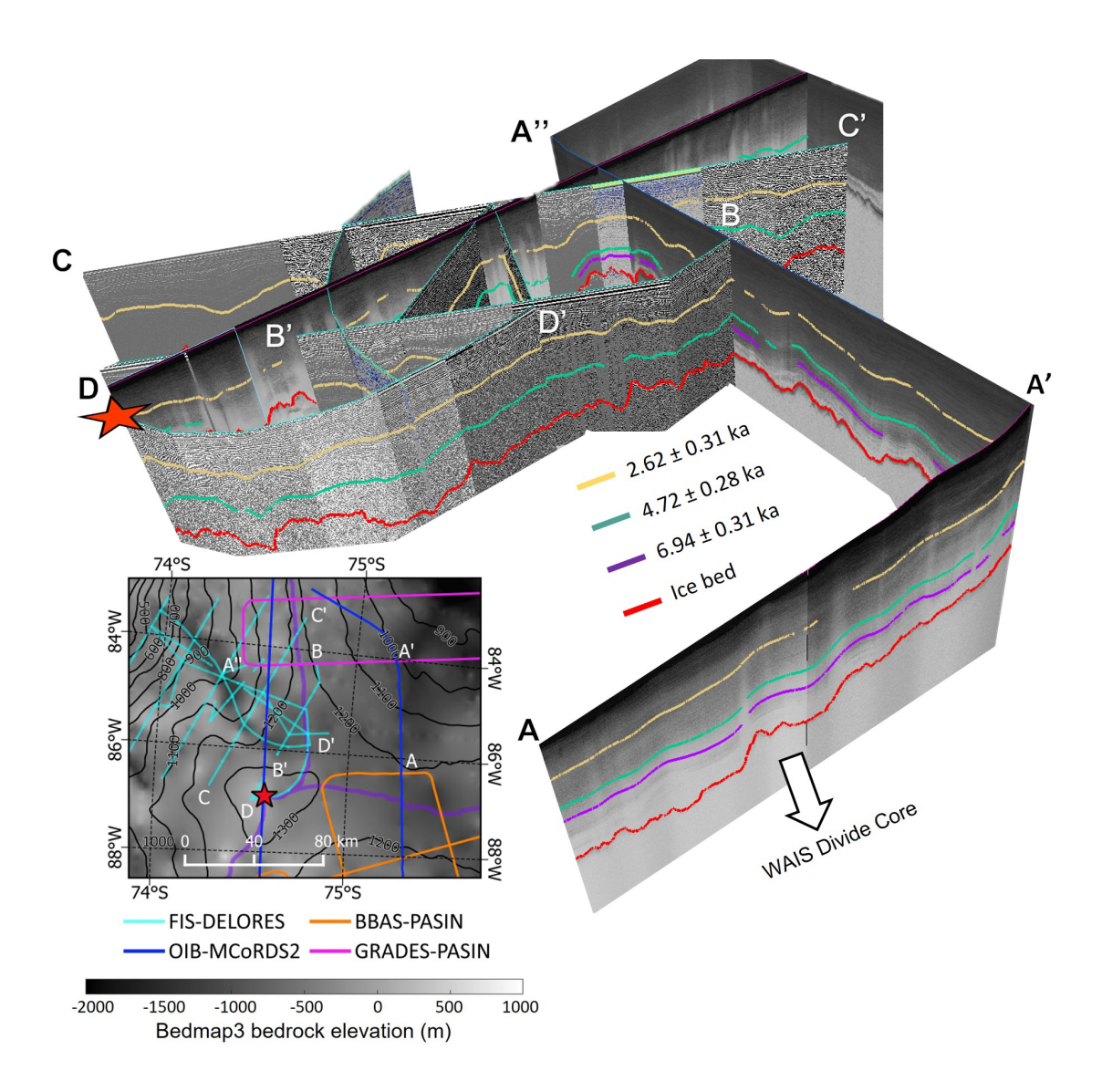


Figure 2. Figure showing a 3-D image of IRHs traced along several intersecting RES profiles from the upper PIG catchment to Ferrigno Ice Stream. RES profiles are orientated looking down Ferrigno Ice Stream towards the Bellingshausen Sea. Inset map (lower left) shows a birds eye view of the RES lines in the 3-D image. The red star in both the inset and enlarged figure correspond to the location of ABW. The ice divides of the Bellingshausen, Amundsen, and Weddell Sea drainage basins are shown in purple (Zwally et al., 2012), with bedrock elevation data from Pritchard et al. (2025), and CryoSat-2 100 m surface-elevation contours from Helm et al. (2014)

can also be readily identified in the OIB-MCoRDS2 RES data (Figure A2), and we thus traced them eastwards along 65 km of a 2018 OIB-MCoRDS2 profile into the Evans Ice Stream catchment (A-A' in Figure 2 and Figure A1). We then continued to trace the three IRHs along the GRADES-PASIN profile for an additional 68 km until the first intersection with the DELORES survey (A'-B in Figure 2). This allowed the 2.62 ka and 4.72 ka IRHs to be extended across large portions of the Ferrigno





Ice Stream catchment, and successfully to the ABW site. However, tracing of the 6.94 ka IRH to ABW, and elsewhere across Ferrigno Ice Stream, was disrupted by steeply dipping topography and elevated ice flow (Bingham et al., 2012).

Appendix A provides detailed information on how each IRH appears across different RES surveys, including key characteristics and uncertainties related to their depths within the ice column.

2.3 Shallow Ice Core Dataset

In December 2010, a 136 m ice core (hereafter termed F10) was drilled at ABW (Thomas et al., 2013, 2015). The F10 core was dated back to 1702, providing a 308-year record of climate variability (Thomas et al., 2013). Snow accumulation was calculated for the entire record using the Nye model (Nye, 1963), and showed a semi-annual cycle, peaking in the autumn and spring (Thomas and Bracegirdle, 2014), with a dramatic increase in accumulation since the onset of the 1900s (Thomas et al., 2015). We use the F10 dataset as a constraint for our inverse model, described in Section 2.4.2, to assess the longer-term changes in accumulation rates.

100 2.4 Model Description

To assess the suitability of a new ice core drilling site, we use a 1-dimensional (1-D) ice flow model, that we will refer to as the forward model, constrained by shallow ice core and dated IRH data to extract surface accumulation records and estimate an age scale for ice at this site. The following section outlines the main principles; Martín et al. (2015) provide the complete numerical derivations.

105 2.4.1 Forward Model

The age of an ice particle derived from our ice-thinning model is based on the principle that an ice particle deposited on the surface of the ice sheet (of ice thickness, H) is then transported with a velocity (u, v, w) through the ice column. As a result, the age of a particle of ice (A) represents the time it takes for a particle of ice to reach a certain position (x, y, z), where z represents the vertical component. If we neglect motion from horizontal advection, the age of an ice particle at a specific depth (d) and time (t) can be expressed as a function of the vertical velocity (w), as shown in Equation 1:

$$\frac{\partial A}{\partial t}(d,t) - w(d,t)\frac{\partial A}{\partial d}(d,t) = 1 \quad 0 \le d \le H,$$

$$-t_0 \le t \le 0,$$

$$A(d,t_0) = A_0,$$

$$A(0,t) = 0.$$
(1)

where A_0 is the initial depth-age, and t_0 is the time before the present t = 0. Assuming the time- and depth-dependency of the vertical velocity component of Equation 1 can be separated, and that there is additionally no basal melting, the vertical velocity is:

115
$$w(d,t) = -\left(a(t) - \frac{\partial H}{\partial t}\right) \frac{\rho_i}{\rho(d)} \eta(d),$$
 (2)





where a is the time-dependent surface accumulation rate, ρ is density, ρ_i is the density of ice, and $\eta(d)$ is the shape function. For simplicity, we assume that there are no changes in ice thickness over time $(\frac{\partial H}{\partial t} = 0)$ and we discuss the implications of this assumption in Section 4.1. Numerically, we solve Equation 1 using a semi-Lagrangian, two-time level, method (Staniforth and Côté, 1991).

As the precise ice-flow conditions at ABW are unknown, we initially use two extreme approximations for the shape function, (1) the Lliboutry approximation (see Equation 3; Lliboutry (1979)) useful for simulating ice thinning at the "flanks" of the ice flow divide, and reproducing ice flow dominated by shear (Martín and Gudmundsson, 2012); and (2) an approximation for representing ice flow at the "divide" from Martín and Gudmundsson (2012).

$$\eta(d) = 1 - \frac{p+2}{p+1} \left(\frac{d}{H}\right) + \frac{1}{p+1} \left(\frac{d}{H}\right)^{p+2},$$
(3)

The Lliboutry parameter *p* in Equation 3 affects the non-linearity of the vertical velocity (Lilien et al., 2021); a higher *p* implies more deformation in the vertical component, and is used to describe the vertical velocity *w* in different "flank" flow regimes. Assumptions associated with the vertical velocity profile include that ice is isotropic (uniform stress and conductivity distribution), and that bedrock variations are smooth.

Our initial model solutions assume that the accumulation rate changes are proportional to the WAIS Divide record (Buizert et al., 2015; Fudge et al., 2016), and we use the advection-corrected accumulation rate from Koutnik et al. (2016), which extends to ~31 ka. As we do not know the precise long-term ice flow conditions at ABW, we hypothesise that ice flow at this point is bounded by both extreme approximations, and so we run the forward models for both "flank" and "divide" ice-flow regimes.

2.4.2 Inverse Model and Optimisation Routines

To date the entire ice column, we formulate an inverse problem of the forward model that assimilates age observations from F10 shallow ice core data (Thomas et al., 2013, 2015) and new dated radar stratigraphy (Section 2.2.2). This approach seeks the optimal records of the accumulation history and ice thinning $(a(t) - \frac{\partial H}{\partial t})$ that minimise the difference between the observed age markers and the modelled age-depth profile (Martín et al., 2015). As we assume that there are no changes in ice thickness through time $(\frac{\partial H}{\partial t} = 0)$, our inversion combines the ice thickness changes with the accumulation history a(t).

To estimate the accumulation rate history between observed time markers, we assume a set of initial solutions for the surface accumulation at ABW that are derived from both the F10 core and IRH data, and then we assume that a(t) is a piecewise linear function and vary the Lliboutry parameter p from 1 to 5 to simulate ice flow at the "flanks". Beyond the deepest observed time marker (a 4.72 ka IRH at 874.1 m), we assume the accumulation rate is proportional to that of the WAIS Divide Ice Core (Buizert et al., 2015; Fudge et al., 2016), and scale the modern accumulation rate estimates from annual layer counting (Thomas et al., 2015) appropriately.

For the optimisation, seeking the piecewise accumulation history that better fits observations, we use a simplex method from Lagarias et al. (1998), as coded in the MATLAB fminsearch function. To avoid over-fitting to the observed F10 and IRH data, we add a regularisation term proportional to the temporal gradient of accumulation ($\frac{\partial a}{\partial t}$) to the difference between





observations and model. We perform L-curve analyses to determine an optimal regularisation parameter (Figure B2) (Hansen, 2000; Wolovick et al., 2023). Small values of the regularisation parameter lead to over-fitting with extreme variations in a(t), while large values of the parameter smooth out any fluctuations in a(t). We then choose an optimal regularisation parameter such that the solution lies between these two extremes (the corner of the L-curve), and derive this mathematically through curvature analysis (Appendix B2) (Wolovick et al., 2023).

2.4.3 Sensitivity to Basal Melting

Our initial optimised solutions are based on the assumption of no basal melting to assess the maximum possible ice record that could be recovered at ABW. We assess the sensitivity of our model to basal melting to thoroughly investigate the suitability of the proposed ice core site.

To do this, we initially used a 1-D steady-state temperature model (Jordan et al., 2018) that, similar to Equation 1, derives the ice temperature at a given depth and time as a function of the vertical velocity. The model is constrained by ice thickness (1,220 m), surface temperature (-20°C) (Thomas and Bracegirdle, 2014), modern accumulation rates (0.33 m/yr) (Thomas et al., 2015), and various geothermal heat flux (GHF) values to calculate a range of basal temperatures. As the GHF across West Antarctica is so poorly constrained (Burton-Johnson et al., 2020; Hazzard and Richards, 2024) and the precise basal conditions at the site are unknown, we ran the temperature model across a wide range of unknown GHF values (50-140 mW/m²) to account for different basal melt regimes. Burton-Johnson et al. (2020) calculated the maximum mean GHF of five continent-scale geophysical estimates to be 106 mW/m² and thus our range of modelled GHF accounts for variations between continent-scale estimates of GHF and their uncertainties.

Under these initial boundary conditions, the model indicates that there will be melting at the bed if the GHF exceeds 67 mW/m² as this is when the basal temperature exceeds 0°C (Figure C1). A detailed breakdown of the steady-state temperature model can be found in Jordan et al. (2018).

Using the values from these simulations, we quantify the basal melting m (Leysinger Vieli et al., 2018) using the following equation:

$$m = \frac{Q_G(x,y) - k_c \frac{\partial T(x,y,d,t)}{\partial d}|_{d=0}}{\rho_w L}$$
(4)

where Q_G is the geothermal heat flux, k_c is the thermal conductivity, L is the latent heat, and ρ_w is the density of water. This calculation of basal melting neglects contributions of heat generated by sliding (horizontal surface velocity is low) and subglacial water flow, and so it is reasonable to assume that GHF would be the largest contributor to melting at the ABW site. We then incorporate the solution to Equation 4 into Equation 2 to assess the sensitivity of the age-depth solution to basal melting.





3 Results

3.1 Geophysical observations

Previous work using the ground-based DELORES survey data identified the presence of a deep subglacial trough running along the centre of Ferrigno Ice Stream (Bingham et al., 2012). The DELORES survey also follows the ice divide and images continuous IRHs and a relatively flat ice-bed interface at the ABW site. The bedrock relief away from the dome at ABW is around 700 m. Coherent layers are imaged in the DELORES data at ABW to around 1,080 m depth, approximately 89 % of the total ice thickness (1,220 m), with layers tending to conform to the bed topography. Although we could only trace two dated IRHs to ABW, there are other traceable layers present above and below the 4.72 ka IRH which, with additional age-depth constraints, could be dated. The elevated accumulation rates at ABW, relative to more inland sites, are likely to produce well-defined annual layers (Palmer et al., 2001) that are effectively imaged by RES, and would provide high-resolution layers within ice-core data.

Mutter and Holschuh (2024) analysed RES data alongside ice-core data at 16 ice-core sites, noting that locations with laterally continuous layers imaged to significant depths in the RES data often provided the most continuous climate records, while sites with larger sections of incoherent scattering were often associated with more disturbed ice-core records. In the DELORES data at ABW, continuous layering is present to 89 % depth with a small region of absent layering, suggesting promising drilling conditions that could allow the recovery of a continuous and undisturbed climate record.

3.2 Accumulation rate history and ice thinning

Figure 3 shows the reconstructed accumulation rates from the inverse model constrained by shallow-ice-core and IRH observations to 4.72 ka, alongside the accumulation rates calculated from the WAIS Divide (Buizert et al., 2015; Fudge et al., 2016) and Dome C (Parrenin et al., 2007) ice cores. We include data from WAIS Divide and Dome C for comparison and to place the ABW ice core in the context of other deep ice cores across the Antarctic Ice Sheet. We indicate in Figure 3 which regions of the solution are constrained by age-depth observations from the F10 core and dated-IRHs, and which regions are scaled to the WAIS Divide accumulation rate record.

There is a peak accumulation rate of \sim 0.75 m yr⁻¹ around 5 ka. The magnitude of this peak accumulation is around 20-30 % higher than the modern accumulation rate estimates from the F10 shallow-ice-core data (Thomas et al., 2015). Comparisons with the WAIS Divide record suggest that the accumulation rates at ABW could be up to three times those measured at WAIS Divide (Figure 3).

During our optimisation routine, we assume that there have been no changes in ice thickness over time (Equation 2: $\frac{\partial H}{\partial t} = 0$) and that changes in the vertical velocity component are entirely influenced by changes in the accumulation regime (a(t)) at ABW. If we relax this assumption and instead assume that the accumulation has been constant over time, we can integrate the output to calculate a rough estimate of the change in ice thickness between the peak in accumulation during the mid-Holocene and the present day. This equates to an approximate 600 m decrease in ice thickness since the mid-Holocene. In reality, we



215



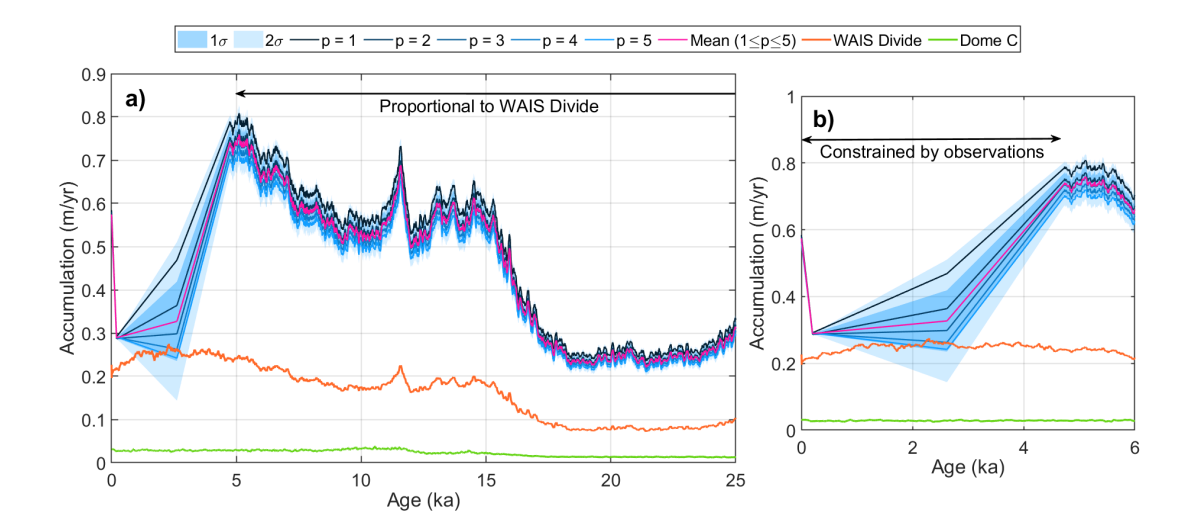


Figure 3. Modelled accumulation rates at the ABW core for different "flank" flow regimes $(1 \le p \le 5)$. Pink line represents the mean across all simulations, orange and green lines correspond to the accumulation records from the WAIS Divide (Buizert et al., 2015; Fudge et al., 2016) and Dome C (Parrenin et al., 2007) ice cores, respectively, and are included on both panels for reference and comparisons in the manuscript. (a) Accumulation rate reconstruction to 25 ka, (b) shows the period where our simulations are constrained by only F10 and dated-IRH observations.

Table 2. Conservative oldest ice estimates, at 90 % and 95 % of the ice thickness, for three optimisations. (1) no basal melting, (2) 10 mm/yr basal melting (67 mW/m²), and (3) 20 mm/yr basal melting (140 mW/m²).

Basal melt (mm/yr)	Ice thickness	Age at 90 % depth (1,098 m)	Age at 95 % depth (1,159 m)
0	1,220 m	11.6 ka	27.0 ka
10	1,220 m	10.5 ka	14.5 ka
20	1,220 m	9.0 ka	11.5 ka

expect that there is a disguised thinning signal in our accumulation rate reconstructions in Figure 3, and that there has been a significant change at ABW over this period, which is an exciting prospect for ice-core drilling.

Figure 3b also highlights the limited number of age constraints available to constrain the accumulation rate reconstructions at this site. This creates some temporal discontinuities in the accumulation rate reconstructions and because our tie points cause a change in the accumulation rate in the model, the precise timing of this change is uncertain and could fall between observations. Furthermore, this results in an inability to pinpoint the onsets of the accumulation changes and/or ice thinning, and would require more age-depth constraints, or an ice core, to minimise this uncertainty.





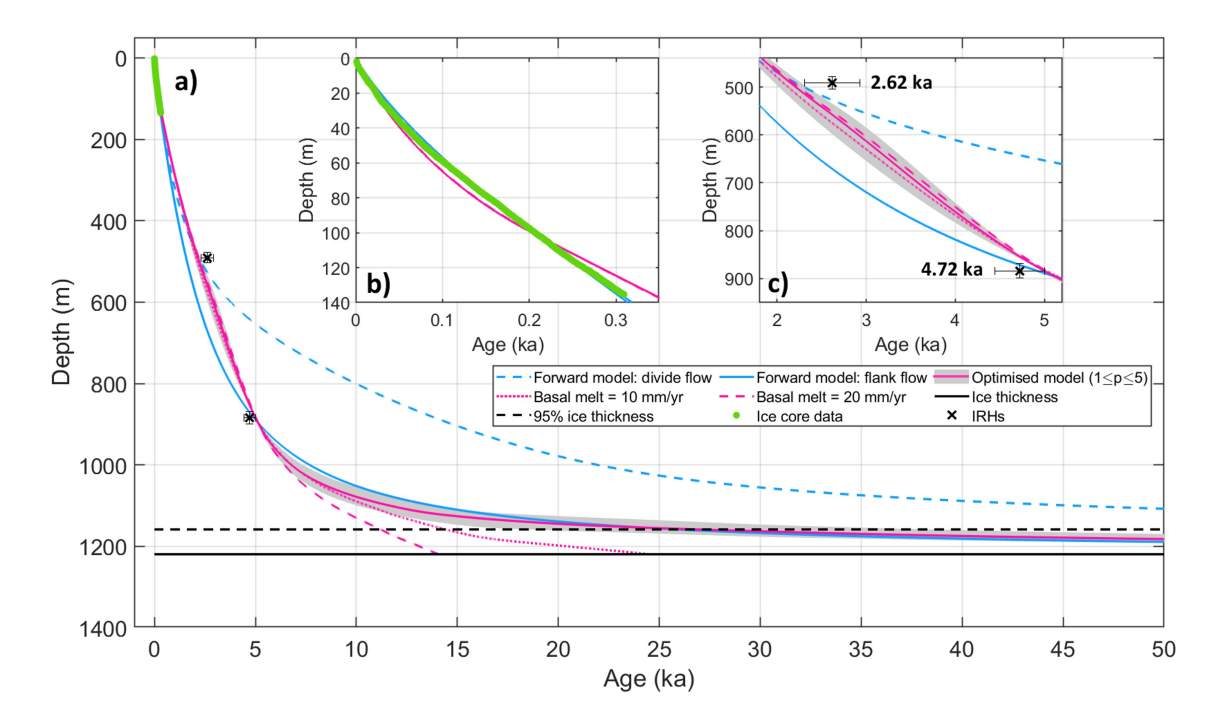


Figure 4. Age-depth profiles from initial forward models (blue lines) and optimised models (pink lines). The solid pink line represents the mean age-depth output from various flank flow simulations ($1 \le p \le 5$), with grey shading indicating the uncertainty between different flank flow regimes. Dashed and dotted pink lines correspond to represent model sensitivity assessments for different basal melt rated scenarios. Age-depth constraints from F10 shallow ice core data (green) and dated-IRHs (black) are indicated by the crosses, with error bars placed on the IRH time markers corresponding to the depth and age uncertainty in these tracings. The dashed black line marks 95 % ice thickness where we infer the age of the oldest ice at ABW, while the solid black line shows the total ice thickness at the ABW site. (a) Age-depth profiles up to 50 ka, (b) zoomed-in age-depth profiles for the period observed with shallow ice core data, (c) zoomed-in age-depth profiles for the dated-IRH period.

3.3 Ice age-depth scale

220

225

Figure 4 shows the modelled age-depth profiles, with associated uncertainties, for the proposed ABW ice core for different basal melt rate scenarios (Table 2). For our no-basal-melt-rate scenario, predicting the age of the ice close to the ice-bed interface is uncertain since the solution to Equation 1 tends to infinity (Figure 4). Furthermore, the model outputs in the deepest parts of the ice column become unrealistic due to their dependence on input parameters. As a result, we take a conservative estimate of the age of the oldest ice at 95 % depth (1159 m - around 60 m above the ice-bed interface, see Table 2). Our results at this depth, when we assume no basal melting (solid pink line in Figure 4), imply that ice ages may be older than the Last Glacial Maximum (Clark et al., 2009), spanning between 18.3 ka and 38.5 ka for different flank flow scenarios. The oldest ice averaged across all "flank" flow simulations at this depth is 27 ka (Figure 4 and Table 2).





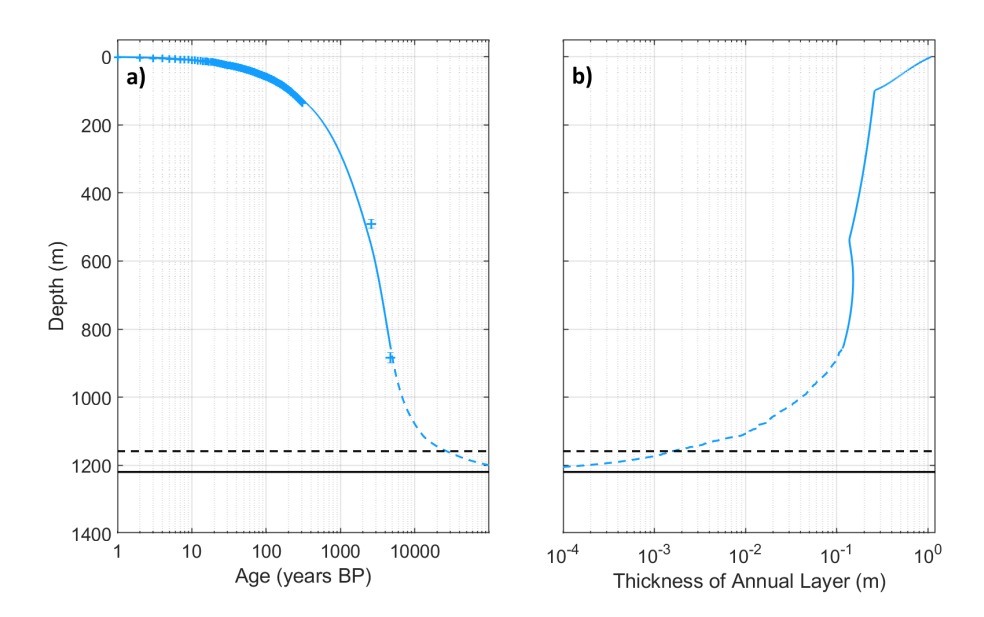


Figure 5. Age and annual layer thickness depth profiles at the ABW site. (a) Optimised age-depth profile from Figure 4 on a log scale. Blue crosses indicate age observations used to constrain the inverse model. (b) Annual layer thickness estimates from the inverse model output. In (a) and (b) blue solid lines indicates where the profiles are constrained by age observations (F10 age data and dated-IRHs; blue crosses), with the dashed blue lines corresponding to where the profiles are constrained by WAIS Divide accumulation data (Buizert et al., 2015; Fudge et al., 2016). Solid and dashed black lines in both panels represent the ice thickness and 95 % depth, respectively, at the ABW site.

The optimised age-depth profile largely follows idealised glacial flow, but we initially prescribe accumulation rates at discrete tie points and assume that the accumulation rate history between observations is a piecewise linear function to find optimal records of accumulation that minimises the difference between the model output and observed time markers (Section 2.4.2). The greatest uncertainty arises in the lower ice column beyond our deepest time marker (4.72 ka) as the uncertainty in the age profile at these depths becomes bounded only by the variable parameter p in Equation 3, and the model assumes that the accumulation rate varies approximately the same as the WAIS Divide ice core record before 4.72 ka.

Figure 5 shows the resolution and layer thickness of the ABW ice core. Assuming annual layers can be resolved down to the centimetre scale (Hoffmann et al., 2022; Grieman et al., 2022), the model output suggests annual layers could be resolved beyond 10 ka. Additionally, at 95 % of the ice thickness, the resolution is \sim 0.64 ka/m, suggesting that the ice at this depth could be both high resolution and highly resolvable, potentially containing a climate record that extends well into the LGP.

3.4 Sensitivity to basal melting

230

235

Incorporating basal melting into model simulations results in greater drawdown of layers in the lowest third of the ice column (Jordan et al., 2018) and, in turn, the age-scale becomes more linear (Figure 4). This reduces the estimated retrievable climate records, at 95 % ice thickness, to 14.5 ka and 11.5 ka under moderate (10 mm/yr: 67 mW/m²) and extremely high (20 mm/yr:





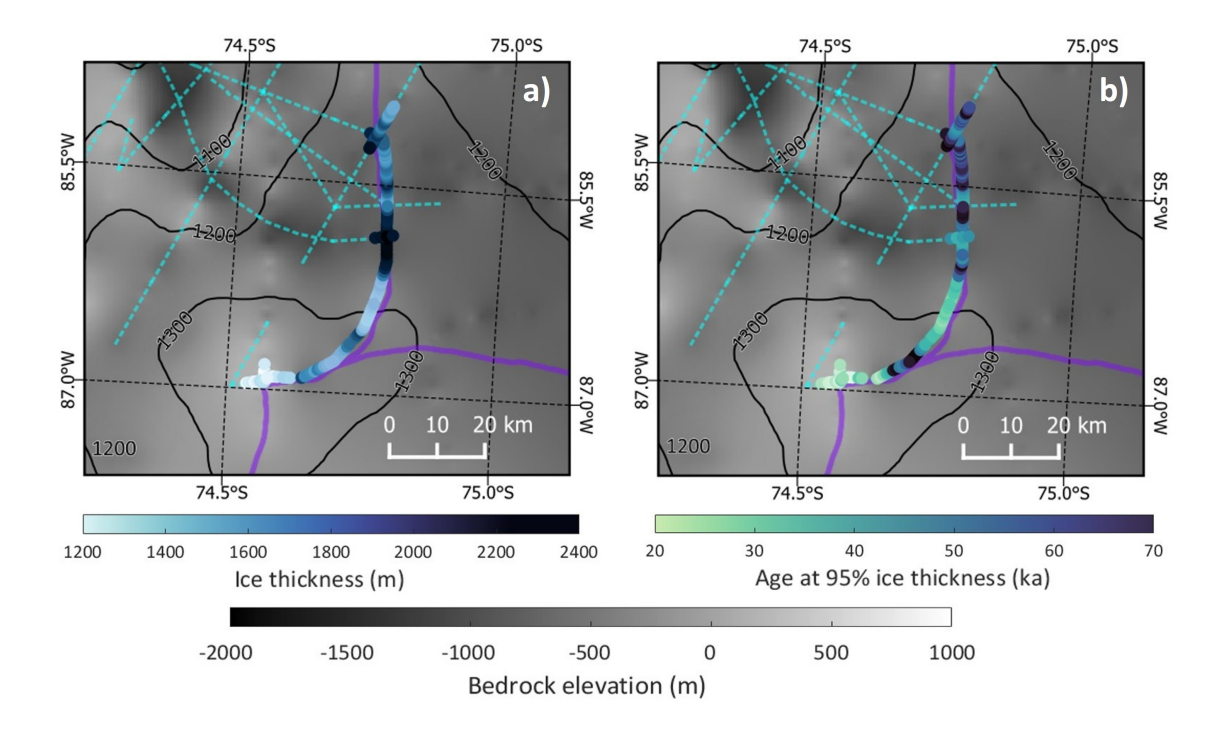


Figure 6. (a) Ice thickness derived from the bed picked in DELORES data, and (b) modelled age of ice at 95 % ice thickness. In both panels: dashed cyan lines represent the DELORES traverse, purple lines outline drainage basin from Zwally et al. (2012), black lines indicate surface elevation contour data from Helm et al. (2014), and data is overlaid on top of bedrock elevation data from Pritchard et al. (2025).

240 140 mW/m²) GHF scenarios (Figure 4 and Table 2). These melt rates are likely overestimated by derivations from an overestimate of the true GHF at ABW. This will in turn underestimate the oldest ice at ABW and hence we treat these simulations as "worse-case" scenarios for basal melting at ABW. Regardless of the actual basal melting values, these results show that a climate record extending beyond the Holocene could still be recovered even if there was some melting at the ice-bed interface.

3.5 Age-depth along the ice divide

Figure 6 displays the modelled age outputs at 95 % ice thickness at ~350 m intervals along the ice divide separating Ferrigno Ice Stream from Pine Island Glacier and Evans Ice Stream. These outputs assume that (1) modern accumulation rates are identical to those at the ABW site (Thomas et al., 2015), (2) flank flow conditions (*p*=3) to account for divergence of the RES traverse from the true divide, and (3) no basal melting. The model is then optimised using new ice thickness and dated-IRHs at intervals along the DELORES divide traverse in Figure 2. In general, we observe older ice in regions of deeper bed topography, but the thickest regions of the divide do not always exhibit the oldest ice (see central divide region of Figure 6). Regions with relatively low ice thickness and older ice, such as the ABW site (Figure 6c), would be more optimal for ice core drilling.

The results of modelling along the DELORES divide traverse highlight the possibility of recovering older ice at locations that offer a thicker ice column. However, comparing the modelled age to the drill depth (ice thickness) (Figure 6c) suggests that





the ABW site offers a valuable climate record for its relatively low drill depth. This makes the ABW site attractive, logistically and financially, as it captures a comprehensive Holocene climate record while minimising drilling time and/or costs, and hence the subsequent environmental impact.

4 Discussion

260

265

270

275

280

285

4.1 Holocene ice thinning

One of the goals of drilling a deep ice core at ABW is to recover a record of ice that can provide information on the onset of ice thinning through the Holocene.

Critically, our modelling has assumed constant ice thickness at the site $(\frac{\partial H}{\partial t} = 0)$ in Equation 2). As a consequence, our model interprets an increase in ice thickness as an increase in accumulation. This is because the ice particles travel faster to their present locations as the ice thickness increases and, with the assumption of constant geometry, the increase in speed is inverted as an increase in accumulation. This raises the question whether the observed changes in accumulation reconstruction (Figure 3) are the result of changes in surface accumulation, ice thinning, or a combination of both, as our method cannot differentiate between them. Although recent changes at ABW have been interpreted as a result of a recent increase in accumulation (Thomas et al., 2015), there have also been reports of ice thinning in the Weddell Sea sector (Grieman et al., 2024) and ice-flow reorganisation around the Ross Ice Shelf area (Kingslake et al., 2018) during the Holocene (Jones et al., 2022). In an area currently experiencing significant changes in ice mass and ice-thinning in the contemporary period (Wouters et al., 2015; Christie et al., 2016; Shepherd et al., 2019; Nilsson et al., 2022), the ABW site, which lies in the coastal area adjacent to the Bellingshausen and Amundsen Seas, is particularly important for reconstructing climatic changes and glacial retreat during the Holocene.

We make several assumptions in our model that could quantitatively vary the results; however, our results strongly suggest that the AWB site has not been in a steady-state (constant accumulation) in the last 5 ka (Figure 3). Our reconstructions also show elevated accumulation relative to other more inland ice cores in West Antarctica (Buizert et al., 2015; Fudge et al., 2016), which implies that the ice recovered could have high resolution and highly resolvable layers (Palmer et al., 2001). Combining this with the drastic change observed between 5-2 ka makes this site attractive for ice-core drilling as the model output suggests a significant change occurred during the mid-Holocene at ABW. Both elevated accumulation rates using radar stratigraphy (Siegert and Payne, 2004; Neumann et al., 2008; Karlsson et al., 2014; Fudge et al., 2016; Koutnik et al., 2016; Bodart et al., 2023) and ice thinning signals from geomorphological, cosmogenic nuclide, and ice-core data (Hein et al., 2016; Grieman et al., 2024) have been observed in other regions of the WAIS during the mid-Holocene. Given the magnitude of the observed decrease in accumulation in Figure 3, it can be inferred that this signal in the model output was likely caused by a combination of both extensive ice thinning and a change in the accumulation regime at ABW.

To resolve climatic changes accurately at ABW, and confirm the signal as an ice-thinning, accumulation rate decrease, or somewhere in between, we need an ice core. Recent work by Grieman et al. (2024) at Skytrain Ice Rise demonstrated the ability to resolve similar signals using ice-core data. In their study, they identified a 450 m ice-sheet thinning signal between



290

295

305

320



8.2 and 8.0 ka and substantial retreat of the ice front between 7.7 and 7.3 ka due to ice-flow changes induced by ungrounding. The maximum change in ice thickness between 5-2 ka at ABW is around 600 m, if we assume that the accumulation rate has remained constant, suggesting that the order of magnitude of the potential ice thinning estimated by the model at ABW is consistent with data from previous deep-ice-core drilling projects in West Antarctica.

The data from the Skytrain Ice Core provided new temporal constraints for ice-sheet models (Mulvaney et al., 2023) and reinforce the importance of these data for resolving major changes to ice-sheet configurations (Wolff et al., 2025). Given the vulnerability of this region to future retreat under the MISI hypothesis (Christie et al., 2016; Miles and Bingham, 2024), an ice core here would greatly improve our understanding of the evolution of the northern Ellsworth Land region of the Antarctic Ice Sheet throughout the Holocene, and provide a more precise timing for the onset of ice-sheet thinning currently observed in satellite data (Shepherd et al., 2019; Nilsson et al., 2022), giving insight into the future stability of the northern Ellsworth Land region.

4.2 Ice core insights

Another goal of drilling a deep ice core at ABW is to recover a comprehensive high-resolution Holocene record of ice (at least 300 11.7 ka), and preferably one that observes the Last Glacial Maximum, that would provide new age-depth constraints for the northern Ellsworth Land region.

Uncertainties in the GHF observations and models (Burton-Johnson et al., 2020; Hazzard and Richards, 2024) at ABW significantly hinder our ability to precisely constrain the age of ice at depth. Instead, we have presented how sensitive our age-depth solution is to basal melting at ABW by testing a wide range of GHF scenarios (50-140 mW/m 2). The solution between 4.72 ka and the present-day is not significantly affected by the addition of basal melting; the age-depth profiles only begin to deviate beyond 6 ka in the lowest regions of the ice column (Jordan et al., 2018) when the GHF exceeds 67 mW/m 2 . Even when we prescribe an extremely high GHF (GHF = 140 mW/m 2), the model still predicts a full-Holocene climate record to be retrievable at ABW.

Under lower basal melt rate scenarios (0-10 mm/yr), the potential recoverable climate record at ABW is between 30-15 ka, showing promise for extending beyond the Holocene and into the LGP. The ice recovered at ABW would provide crucial data for resolving the onsets of the dynamic thinning and retreat currently observed along the Bellingshausen Sea coastline and placing recent thinning observations from the Skytrain Ice Rise ice core (Grieman et al., 2024) in the context of the wider northern Ellsworth Land region.

While ABW hence presents an opportunity to recover a climate record that exceeds the onset of the Holocene (Figure 4), the ice layers must be interpretable and coherent for analysis (Mutter and Holschuh, 2024). Figure 5 suggests that annual layers could be recovered to around 7 ka (assuming that layers of 5 cm thickness can be resolved), and that the ABW core would have a high layer resolution of 0.58 ka m⁻¹ at 95 % depth. In addition, DELORES data at ABW show coherent layers present to around 90 % depth. Through recent work performed by Mutter and Holschuh (2024) evaluating RES data at ice-core sites, our observations of coherent layers spanning most of the ice column suggest that the ice-core record could be undisturbed to within 100 m of the ice-bed interface. Achieving an undisturbed Holocene climate record would provide the longest climate record in





the Bellingshausen Sea Sector and also provide a unique set of constraints for ice-sheet models. Better constraints in ice-sheet models improve reconstructions of past ice-sheet configurations (Wolff et al., 2025), which in turn benefits modelling future projections of ice mass loss in northern Ellsworth Land and our understanding of the long-term (in)stability and interglacial variability of marine basins in West Antarctica.

325 4.3 Outlook

330

335

340

345

350

The novelty of our modelling approach lies in its ability to integrate modern accumulation constraints from shallow-ice-core data with new age-depth observations from dated IRHs. This constrains the optimisation procedure, allowing us to find optimal records of the long-term accumulation rates at ABW that extend beyond the limits of estimates from contemporary datasets. Consequently, the model can be easily applied to new sites near ice divides, where horizontal ice flow is negligible and where we have age-depth constraints spanning the whole ice column, offering exciting prospects for the ice coring community.

To improve the performance of the model, precise age observations at depth and accurate estimates of modern accumulation rates are essential. In West Antarctica, dating constraints are often limited to the WAIS Divide and Byrd ice cores (Bodart et al., 2021), resulting in fewer dated IRHs to constrain model outputs in regions far from these ice cores (Bingham et al., 2025). To obtain new constraints for dating new layers in the lower ice column, we need new strategically located deep ice cores. These ice cores should ideally (1) provide climatic records preceding the Holocene and the LGP to allow dating of layers in the lower ice column, and (2) be situated in areas with high layer continuity. The latter is progressively being informed by the AntArchitecture initiative's steady build-up of a 3-D age-depth structure for the Antarctic Ice Sheet (Bingham et al., 2025).

An increased number of age-depth observations would provide more data to constrain the optimisation routine in Section 2.4.2 and, in turn, reduce the temporal discontinuities in the accumulation-rate reconstructions observed in Figure 3. This would improve our ability to constrain the timing of this inferred change in the accumulation rate observed between 4.72 ka and present day, and help to better resolve the onset of the inferred dramatic ice thinning in northern Ellsworth Land. Understanding the longer-term changes in more detail is essential to understand whether the contemporary observations of ice thinning are part of recurring periods of thinning, retreat and advance, or whether there is a significant concern of rapid irreversible retreat in the future. An ice core at ABW would provide a new high-resolution climate record essential for answering questions on the long-term history of the northern Ellsworth Land region of the Antarctic Ice Sheet, and how this region may contribute to future sea-level rise.

5 Conclusions

We have evaluated the suitability of the triple-ice divide point between the Amundsen, Bellingshausen, and Weddell Seas (ABW; 74°34'37S, 86°54'16W) as a site to recover an ice core that may better elucidate the Holocene history of the region.

The ice is approximately 1200 m thick, with coherent internal layers imaged by radio-echo sounding up to 100 m above the ice-bed interface. Although the precise geothermal heat flux is unknown, modelling indicates that basal melting begins at 67



355

360

365

370

375

380



mW/m². By assimilating age observations from shallow-ice-core data and new dated radar stratigraphy in a one-dimensional ice-thinning model, we estimated records of accumulation and derived an age scale for ice at the site.

We have shown that we can better constrain the long-term accumulation rate history using radar stratigraphy data, and these observations reveal a significant shift in the accumulation regime and ice thickness at ABW between 5-2 ka. The accumulation rate reconstructions and the age scale suggest that the ice core would provide a high-resolution climate record extending beyond the onset of the Holocene. Our best-fit age-depth scale shows ice up to 27 ka at 95 % of the ice thickness, with annual layers at this depth a few millimetres thick, showing promise for recovering a climate record exceeding 30 ka. This location shows promise for deep ice coring and could precisely resolve the timing of ice thinning in this data-poor region of West Antarctica and significantly improve our understanding of the climatic changes and glacial retreat in northern Ellsworth Land during the Holocene.

Appendix A: IRH Tracing

A1 Methods

We continuously traced the three IRHs along approximately 65 km of the 2018 OIB-MCoRDS2 survey before intersecting the GRADES-PASIN G04 profile (Figure 2: A-A'). Figure A1 shows how the IRHs appear in the higher frequency MCoRDS2 survey, and Figure A2 shows how the IRHs manifest at the intersection (A' in Figure 2) of the GRADES-PASIN and OIB-MCoRDS2 flights. The 4.72 ka IRH is distinctly bright in the OIB-MCoRDS2 data; the 2.62 ka IRH is a bright reflector among several other bright reflectors, while the 6.94 ka IRH lies just above another single bright reflector, resulting in a distinct doublet of layers that can be tracked across the whole profile in Figure A1 (the shallowest of the doublet represents the 6.94 ka IRH, and is the one we trace).

Shortly after commencing IRH tracing in the DELORES data (around 7 km from the intersection towards the central trough of Ferrigno Ice Stream), the deepest IRH (6.94 ka) becomes disrupted due to steeply dipping bed topography (Bingham et al., 2012). As a result, the layer is no longer imaged (max angle around 10 degrees for imaging reflectors in DELORES, (Cavitte et al., 2021)). This rapid change in bed elevation means that the 6.94 ka IRH approaches a depth at which reflections are obscured by noise in the DELORES data, and thus we are forced stop tracing the 6.94 ka IRH here. Both of the 2.62 ka and 4.72 ka IRHs can be continuously traced upstream of Ferrigno Ice Stream catchment and in the slower-flowing regions of the main ice stream (Figure 2 and Figure A3). Most importantly, both IRHs reach ABW where the F10 shallow-ice-core is located, allowing new and deeper age constraints to be used in the modelling work described in Section 2.4.2.

Figure A3 shows the fractional depths of the 2.62 ka and 4.72 ka IRHs across the Ferrigno Ice Stream catchment, averaging 39.9 % and 68.2 %, respectively. The 2.62 ka IRH was slightly more extensive than the 4.72 ka IRH across the Ferrigno Ice Stream catchment due to the ability to trace the 2.62 ka IRH across the upper part of the trough in Figure A3. The central trough of Ferrigno Ice Stream (Bingham et al., 2012) largely disrupts the IRH tracing due to both elevated ice flow and steeply dipping reflectors from layer drawdown at the onset of the trough.





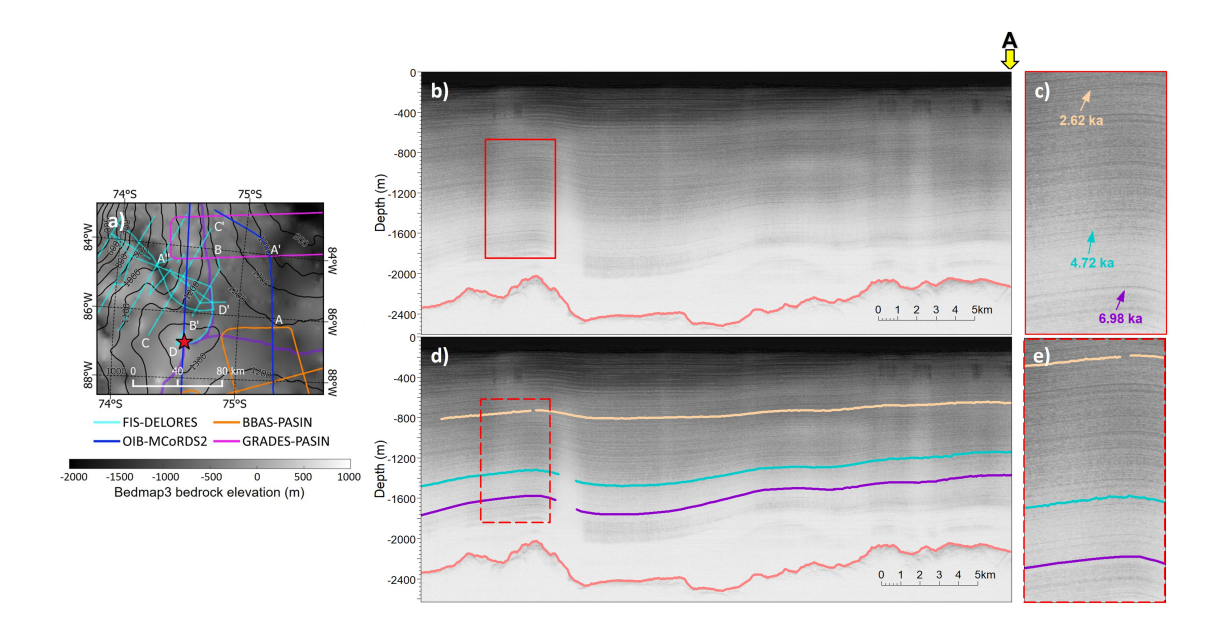


Figure A1. RES profiles showing the location of the onset of IRH tracing in this study, with zoomed views (c,e) highlighting the appearance of the three traced IRHs in more detail. (a) Map of the study area, highlighting key RES datasets used in this study and the ABW site (red star), overlaid on bedrock elevation data from Pritchard et al. (2025), and CryoSat-2 100 m surface-elevation contours from Helm et al. (2014). The ice divides of the Bellingshausen, Amundsen, and Weddell Sea drainage basins are shown in purple (Zwally et al., 2012). (b)-(e) OIB-MCoRDS2 RES profiles at the intersection (A) with the BBAS-PASIN flight-line, illustrating the appearance of IRHs in the OIB-MCoRDS2 data and their manifestation along the flight-line.

A2 Uncertainties

All of the IRHs were traced in the TWT time domain and converted to depth below the ice surface using a frequently-used electromagnetic wave speed of 168.5 m μs⁻¹. As the wave speed varies between 168 and 169.5 m μs⁻¹ through the ice column (Fujita et al., 2000), we assume that the uncertainty in wave speed is ±2 m μs⁻¹ (Koutnik et al., 2016), and we calculate uncertainties of 5.7 m for the 2.62 ka IRH and 10.4 m for the 4.72 ka IRH based on this. We also account for the uncertainty arising from the different wave propagation rates through firn and ice (Dowdeswell and Evans, 2004), and employ a firn correction of +10 m in the vertical direction with an uncertainty of ±3 m (Lilien et al., 2021), which has been used widely across other studies in West Antarctica (Ross et al., 2012; Siegert et al., 2013; Ashmore et al., 2020; Bodart et al., 2021). Combining the uncertainties described above with those arising from the vertical resolution of each system (see Table 1; (Cavitte et al., 2016; King, 2020)), we summed these contributions in quadrature to yield total uncertainties of approximately 12.9 m and 15.5 m for the 2.62 ka and 4.72 ka IRH, respectively.





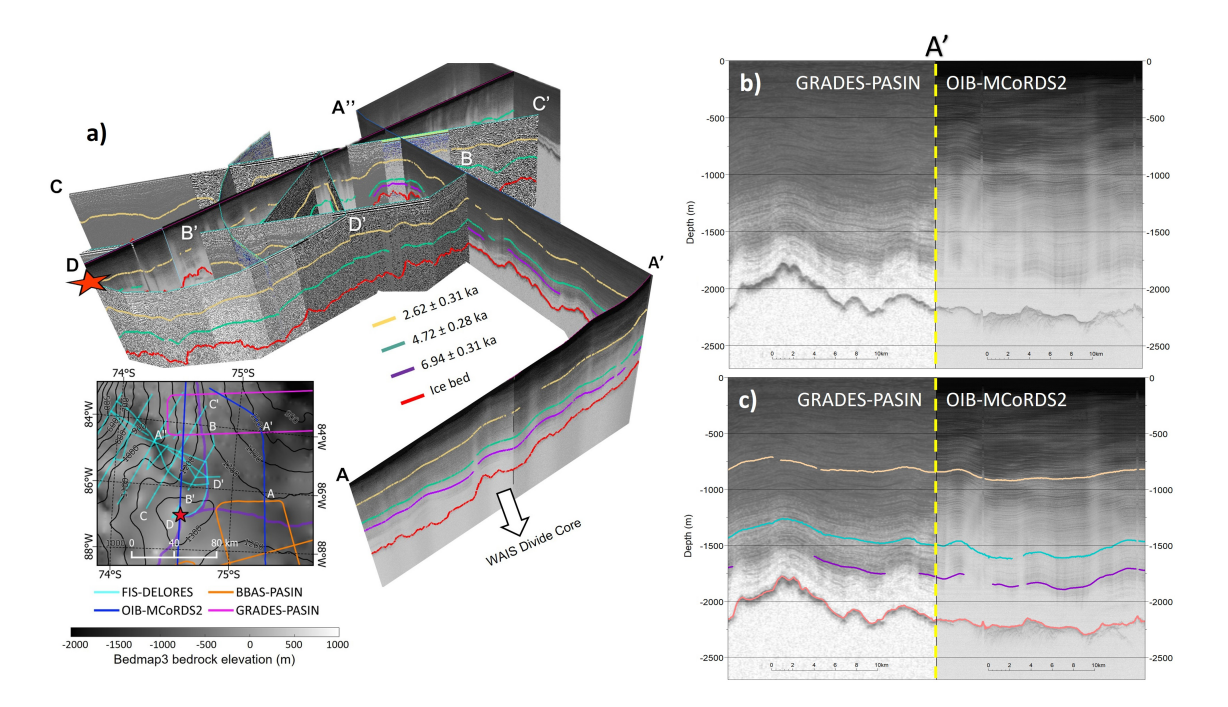


Figure A2. Zoomed-in view of the intersection (A') between the OIB-MCoRDS2 and GRADES-PASIN RES flight-lines. (a) Figure 2 from the main text. (b)-(c) RES profiles at the crossover between GRADES-PASIN (on the left) and OIB-MCoRDS2 (on the right) without (b) and with IRH traces (c).

395 Appendix B: Cost function and L-curves

The inverse problem is Section 2.4.2 is formulated as finding optimal records of accumulation a(t) that minimise the difference between observations and modelled results. To prevent the model overfitting to the observational data, we conduct L-curve analyses to determine an optimal regularisation parameter following a mathematical approach similar to the one described in Wolovick et al. (2023).

400 B1 Cost function

In our cost function, we use a single observational misfit and a single regularisation term. Our observational misfit (J_{obs}) is defined as the mean square error between the observed ages and the modelled age outputs.

$$J_{obs} = \frac{1}{n} \sum_{i=1}^{n} (A(d_i, t_i) - A_{obs, i})^2$$
(B1)

where $A_{obs,i}$ is the observed age, A is the modelled age at depth d and time t, and n represents the number of observations.

To penalise high variability between modelled accumulation rate outputs, we employ a regularisation term (J_{reg}) which is the





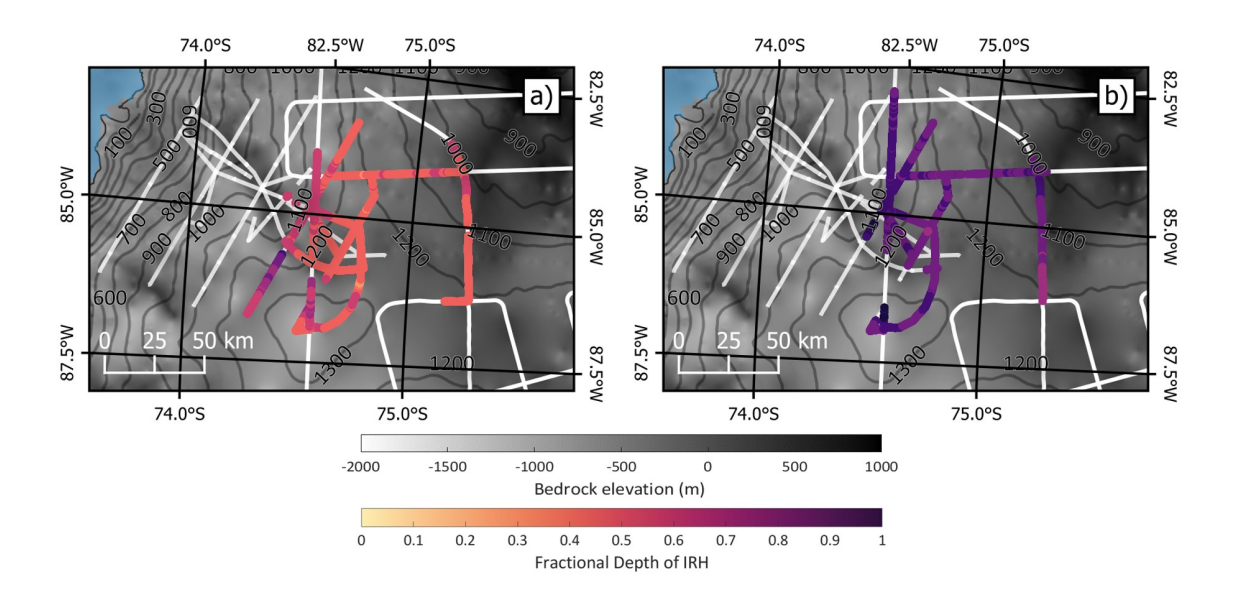


Figure A3. Fractional depths of the 2.62 ka (a) and 4.72 ka (b) IRHs across the Ferrigno Ice Stream catchment. Bedrock elevation data is from Pritchard et al. (2025), and CryoSat-2 100 m surface-elevation contours come from Helm et al. (2014)

standard deviation (σ) of the values of a at the tie-points (a_{opt}) in the piecewise linear function (Section 2.4.2).

$$J_{reg} = \sigma(a_{opt}) \tag{B2}$$

The total cost function (J) that is minimised to find optimal records of accumulation, a(t), in Section 2.4.2 is:

$$J = J_{obs} + \lambda J_{reg} \tag{B3}$$

where λ denotes the weight of the Tikhonov regularisation parameter for accumulation. We run the inverse model for a range of λ values and find an optimal range of λ values through L-curve analyses.

B2 L-curves

In Figure B1a, we plot the values of J_{obs} and J_{reg} together in log-log space and a visible "L" can be observed for the range of modelled λ values. An immediate visual inspection of Figure B1a highlights a range of possible λ values at the corner of the L-curve. For large values of λ , the curve becomes horizontal and the age-depth solution is over-smoothed; this is explicitly shown in Figure B1c where the gradients of both costs become constant for large λ values. For small λ values the age-depth solution overfits to the input observations, and J_{obs} is small, so finding an optimal λ value between both of these extremes is crucial to appropriately control the output solution.

To determine an optimal λ value, we compute the first derivatives (Figure B1c) and second (Figure B1d) derivatives of both the observational and regularisation components of the cost function. We then sum the cost curvatures for each component of the cost function to derive the total curvature. The location of the maximum total curvature ($\lambda = \sim 12,500$) represents





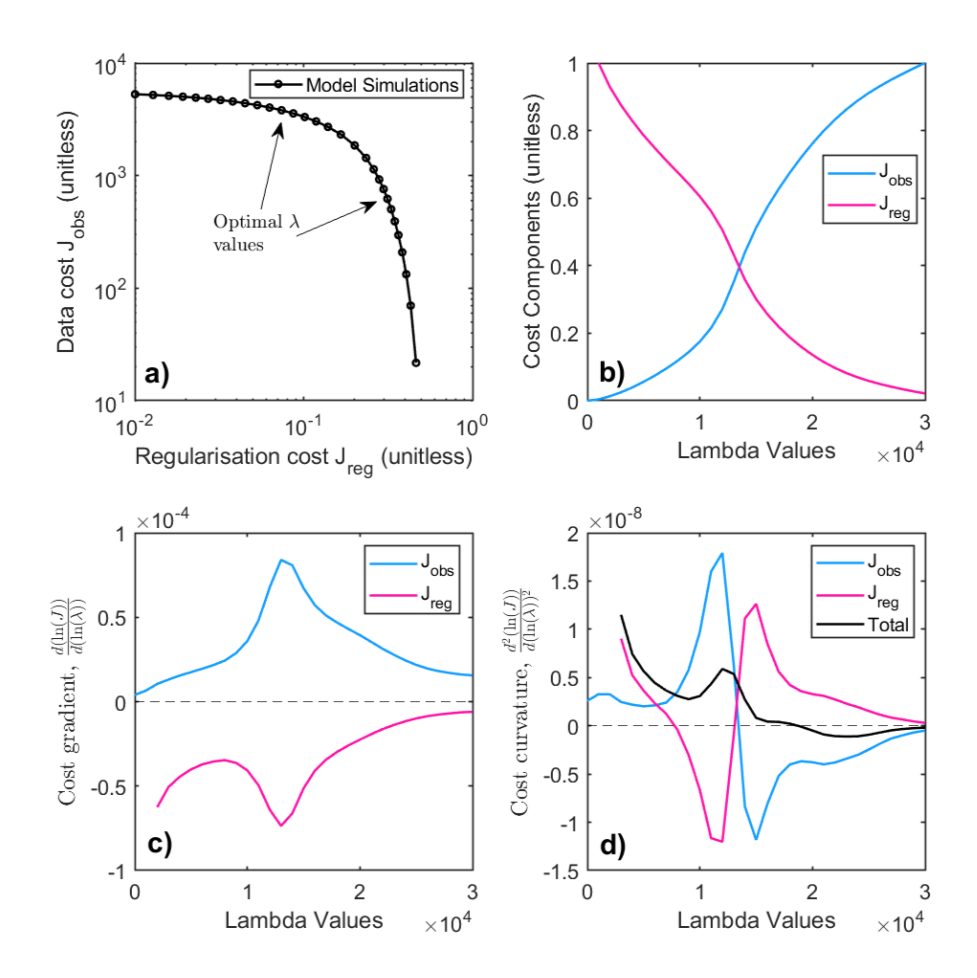


Figure B1. L-curve regularisation to minimise over-fitting to observational data. (a) L-curve from log-log plot of J_{obs} vs J_{reg} . Black circles represent the sampled lambda values, with the red arrows identifying the corner of the L-curve. (b) Plot of both components in the cost function. (c) and (d) represent the cost gradient and cost curvature, respectively, as a function of lambda. Our optimal lambda values $(\lambda = 12,500)$ sits at the location of maximum curvature in (d).

the location of the sharpest corner in the L-curve, and thus the optimal λ value. We select this value to use in our model simulations, but a range of λ values where the curvature is greater than half the maximum curvature would likely also be acceptable (Wolovick et al., 2023).

425 cost gradient =
$$\frac{d(\ln(J))}{d(\ln(\lambda))}$$
 (B4)

$$cost curvature = \frac{d^2(\ln(J))}{d(\ln(\lambda))^2}$$
(B5)



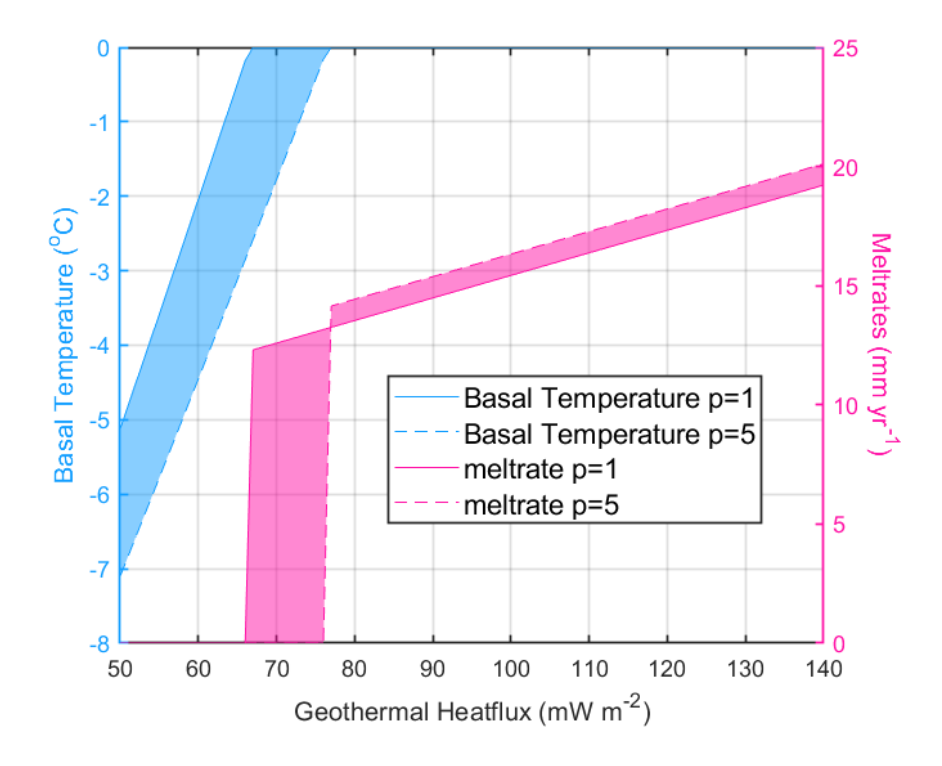


Figure C1. Estimates of basal temperatures derived using a steady-state temperature model (Section 2.4.3) and basal melt rates (calculated with Equation 4) for a range of geothermal heat flux values at ABW. The onset of melting at ABW occurs at 67 mW/m².

Appendix C: Basal melt results

430

435

In order to estimate the basal melting at the ABW site, where we cannot constrain the precise GHF, we adopt an approach to estimate basal melt rates from an ice temperature profile estimated using a steady-state temperature model detailed in Jordan et al. (2018). This model calculates the ice temperature at a given depth and time as a function of the vertical velocity similar to the age-depth model described in Section 2.4.1. As the GHF at ABW is poorly-constrained (Burton-Johnson et al., 2020), we constrain the model using a range of GHF values (50-140 mW/m 2) to account for discrepancies between individual GHF data products. We then extract the basal temperature output and calculate melting using Equation 4 (Leysinger Vieli et al., 2018). The temperature profiles at ABW indicate that the onset of basal melting (when basal temperatures rise above $0^{\circ}C$) initiates at 67 mW/m 2 (Figure C1). We calculate melt rates for these conditions to be around 10 mm/yr, rising up to 20 mm/yr for the highest GHF (140 mW/m 2).

In Section 4.2, we discuss how prescribing these melt rates influences the modelled age-depth profiles at ABW.





Data availability. The 1-D age-depth model, the resulting age-depth and accumulation outputs, and the code used to analyse and plot the data provided in this manuscript are freely available on GitHub (https://github.com/harryjoedavis/ABW_ice_core) and archived on Zenodo.

440 The new dated IRH dataset generated across northern Ellsworth Land, and used to constrain the 1-D model, is archived on Zenodo.

Competing interests. C.M is a member of the editorial board of *The Cryosphere*.

Acknowledgements. This study was motivated by the Scientific Committee for Antarctic Research's Action Group AntArchitecture. The authors gratefully acknowledge British Antarctic Survey Scientific and Operations personnel for supporting the acquisition of airborne (PASIN) and ground-based (DELORES) RES data, and NASA/Operation IceBridge/University of Kansas personnel under the auspices of the U.S. National Science Foundation (NSF) Center for Remote Sensing of Intergrated Systems (CReSIS) for acquiring MCoRDS2 airborne RES data, across northern Ellsworth Land. Chris Griffiths provided invaluable field assistance for the 2009/10 Ferrigno Ice Stream RES campaign. The authors also gratefully acknowledge the European Space Agency and the European Commission for the acquisition, generation, and availability of Copernicus Sentinel-1 data.

Financial support. The research was supported by the Natural Environment Research Council (NERC) Satellite Data in Environmental Science (SENSE) Centre for Doctoral Training PhD Scholarship awarded to H.J.D under the supervision of R.G.B, A.S.H, and A.E.H (grant no. NE/T00939X/1). E.R.T and C.M were supported by NERC (grant no. NE/W001535/1). A.E.H was supported by ESA through the 5-D Antarctica project (4000146702/24/I-KE).





References

- Alley, R. B., Anandakrishnan, S., Christianson, K., Horgan, H. J., Muto, A., Parizek, B. R., Pollard, D., and Walker, R. T.:

 Oceanic Forcing of Ice-Sheet Retreat: West Antarctica and More, Annual Review of Earth and Planetary Sciences, 43, 207–231, https://doi.org/https://doi.org/10.1146/annurev-earth-060614-105344, 2015.
 - Arnold, E., Leuschen, C., Rodriguez-Morales, F., Li, J., Paden, J., Hale, R., and Keshmiri, S.: CReSIS airborne radars and platforms for ice and snow sounding, Annals of Glaciology, 61, 58–67, https://doi.org/10.1017/aog.2019.37, 2020.
- Ashmore, D. W., Bingham, R. G., Hindmarsh, R. C. A., Corr, H. F. J., and Joughin, I. R.: The relationship between sticky spots and radar reflectivity beneath an active West Antarctic ice stream, Annals of Glaciology, 55, 29–38, https://doi.org/10.3189/2014AoG67A052, 2014.
 - Ashmore, D. W., Bingham, R. G., Ross, N., Siegert, M. J., Jordan, T. A., and Mair, D. W. F.: Englacial Architecture and Age-Depth Constraints Across the West Antarctic Ice Sheet, Geophysical Research Letters, 47, e2019GL086 663, https://doi.org/10.1029/2019GL086663, 2020.
- Bentley, M. J., Ó Cofaigh, C., Anderson, J. B., Conway, H., Davies, B., Graham, A. G. C., Hillenbrand, C.-D., Hodgson, D. A., Jamieson, S. S. R., Larter, R. D., Mackintosh, A., Smith, J. A., Verleyen, E., Ackert, R. P., Bart, P. J., Berg, S., Brunstein, D., Canals, M., Colhoun, E. A., Crosta, X., Dickens, W. A., Domack, E., Dowdeswell, J. A., Dunbar, R., Ehrmann, W., Evans, J., Favier, V., Fink, D., Fogwill, C. J., Glasser, N. F., Gohl, K., Golledge, N. R., Goodwin, I., Gore, D. B., Greenwood, S. L., Hall, B. L., Hall, K., Hedding, D. W., Hein, A. S., Hocking, E. P., Jakobsson, M., Johnson, J. S., Jomelli, V., Jones, R. S., Klages, J. P., Kristoffersen, Y., Kuhn, G., Leventer, A., Licht, K., Lilly, K., Lindow, J., Livingstone, S. J., Massé, G., McGlone, M. S., McKay, R. M., Melles, M., Miura, H., Mulvaney, R., Nel,
- W., Nitsche, F. O., O'Brien, P. E., Post, A. L., Roberts, S. J., Saunders, K. M., Selkirk, P. M., Simms, A. R., Spiegel, C., Stolldorf, T. D., Sugden, D. E., van der Putten, N., van Ommen, T., Verfaillie, D., Vyverman, W., Wagner, B., White, D. A., Witus, A. E., and Zwartz, D.: A community-based geological reconstruction of Antarctic Ice Sheet deglaciation since the Last Glacial Maximum, Quaternary Science Reviews, 100, 1–9, https://doi.org/10.1016/j.quascirev.2014.06.025, 2014.
- Bingham, R. G., Ferraccioli, F., King, E. C., Larter, R. D., Pritchard, H. D., Smith, A. M., and Vaughan, D. G.: Inland thinning of West

 Antarctic Ice Sheet steered along subglacial rifts, Nature, 487, 468–471, https://doi.org/10.1038/nature11292, 2012.
 - Bingham, R. G., Bodart, J. A., Cavitte, M. G. P., Chung, A., Sanderson, R. J., Sutter, J. C. R., Eisen, O., Karlsson, N. B., MacGregor, J. A., Ross, N., Young, D. A., Ashmore, D. W., Born, A., Chu, W., Cui, X., Drews, R., Franke, S., Goel, V., Goodge, J. W., Henry, A. C. J., Hermant, A., Hills, B. H., Holschuh, N., Koutnik, M. R., Leysinger Vieli, G. J.-M. C., MacKie, E. J., Mantelli, E., Martín, C., Ng, F. S. L., Oraschewski, F. M., Napoleoni, F., Parrenin, F., Popov, S. V., Rieckh, T., Schlegel, R., Schroeder, D. M., Siegert, M. J., Tang, X., Teisberg,
- T. O., Winter, K., Yan, S., Davis, H., Dow, C. F., Fudge, T. J., Jordan, T. A., Kulessa, B., Matsuoka, K., Nyqvist, C. J., Rahnemoonfar, M., Siegfried, M. R., Singh, S., Višnjević, V., Zamora, R., and Zuhr, A.: Review article: AntArchitecture building an age–depth model from Antarctica's radiostratigraphy to explore ice-sheet evolution, The Cryosphere, 19, 4611–4655, https://doi.org/10.5194/tc-19-4611-2025, 2025.
- Bodart, J. A., Bingham, R. G., Ashmore, D. W., Karlsson, N. B., Hein, A. S., and Vaughan, D. G.: Age-Depth Stratigraphy of Pine Island

 Glacier Inferred From Airborne Radar and Ice-Core Chronology, Journal of Geophysical Research: Earth Surface, 126, e2020JF005927, https://doi.org/10.1029/2020JF005927, 2021.
 - Bodart, J. A., Bingham, R. G., Young, D. A., MacGregor, J. A., Ashmore, D. W., Quartini, E., Hein, A. S., Vaughan, D. G., and Blankenship, D. D.: High mid-Holocene accumulation rates over West Antarctica inferred from a pervasive ice-penetrating radar reflector, The Cryosphere, 17, 1497–1512, https://doi.org/10.5194/tc-17-1497-2023, 2023.



505



- Buizert, C., Cuffey, K. M., Severinghaus, J. P., Baggenstos, D., Fudge, T. J., Steig, E. J., Markle, B. R., Winstrup, M., Rhodes, R. H., Brook, E. J., Sowers, T. A., Clow, G. D., Cheng, H., Edwards, R. L., Sigl, M., McConnell, J. R., and Taylor, K. C.: The WAIS Divide deep ice core WD2014 chronology Part 1: Methane synchronization (68–31 ka BP) and the gas age–ice age difference, Climate of the Past, 11, 153–173, https://doi.org/10.5194/cp-11-153-2015, 2015.
- Burton-Johnson, A., Dziadek, R., and Martin, C.: Review article: Geothermal heat flow in Antarctica: current and future directions, The Cryosphere, 14, 3843–3873, https://doi.org/10.5194/tc-14-3843-2020, 2020.
 - Cavitte, M. G. P., Blankenship, D. D., Young, D. A., Schroeder, D. M., Parrenin, F., Lemeur, E., Macgregor, J. A., and Siegert, M. J.: Deep radiostratigraphy of the East Antarctic plateau: connecting the Dome C and Vostok ice core sites, Journal of Glaciology, 62, 323–334, https://doi.org/10.1017/jog.2016.11, 2016.
- Cavitte, M. G. P., Young, D. A., Mulvaney, R., Ritz, C., Greenbaum, J. S., Ng, G., Kempf, S. D., Quartini, E., Muldoon, G. R., Paden,
 J., Frezzotti, M., Roberts, J. L., Tozer, C. R., Schroeder, D. M., and Blankenship, D. D.: A detailed radiostratigraphic data set for the central East Antarctic Plateau spanning from the Holocene to the mid-Pleistocene, Earth System Science Data, 13, 4759–4777, https://doi.org/10.5194/essd-13-4759-2021, 2021.
 - Christie, F. D. W., Bingham, R. G., Gourmelen, N., Tett, S. F. B., and Muto, A.: Four-decade record of pervasive grounding line retreat along the Bellingshausen margin of West Antarctica, Geophysical Research Letters, 43, 5741–5749, https://doi.org/10.1002/2016GL068972, 2016.
 - Clark, P. U., Dyke, A. S., Shakun, J. D., Carlson, A. E., Clark, J., Wohlfarth, B., Mitrovica, J. X., Hostetler, S. W., and McCabe, A. M.: The Last Glacial Maximum, Science, 325, 710–714, https://doi.org/10.1126/science.1172873, 2009.
 - Corr, H.: Processed airborne radio-echo sounding data from the GRADES-IMAGE survey covering the Evans and Rutford Ice Streams, and ice rises in the Ronne Ice Shelf, West Antarctica (2006/2007), https://doi.org/https://doi.org/10.5285/c7ea5697-87e3-4529-a0dd-089a2ed638fb, 2021.
 - CReSIS: MCoRDS2 Data, http://data.cresis.ku.edu/, 2024.
 - Dowdeswell, J. A. and Evans, S.: Investigations of the form and flow of ice sheets and glaciers using radio-echo sounding, Reports on Progress in Physics, 67, 1821, https://doi.org/10.1088/0034-4885/67/10/R03, 2004.
- Edwards, T. L., Nowicki, S., Marzeion, B., Hock, R., Goelzer, H., Seroussi, H., Jourdain, N. C., Slater, D. A., Turner, F. E., Smith, C. J.,

 McKenna, C. M., Simon, E., Abe-Ouchi, A., Gregory, J. M., Larour, E., Lipscomb, W. H., Payne, A. J., Shepherd, A., Agosta, C.,

 Alexander, P., Albrecht, T., Anderson, B., Asay-Davis, X., Aschwanden, A., Barthel, A., Bliss, A., Calov, R., Chambers, C., Champollion,

 N., Choi, Y., Cullather, R., Cuzzone, J., Dumas, C., Felikson, D., Fettweis, X., Fujita, K., Galton-Fenzi, B. K., Gladstone, R., Golledge,

 N. R., Greve, R., Hattermann, T., Hoffman, M. J., Humbert, A., Huss, M., Huybrechts, P., Immerzeel, W., Kleiner, T., Kraaijenbrink, P.,

 Le clec'h, S., Lee, V., Leguy, G. R., Little, C. M., Lowry, D. P., Malles, J.-H., Martin, D. F., Maussion, F., Morlighem, M., O'Neill, J. F.,
- Nias, I., Pattyn, F., Pelle, T., Price, S. F., Quiquet, A., Radić, V., Reese, R., Rounce, D. R., Rückamp, M., Sakai, A., Shafer, C., Schlegel, N.-J., Shannon, S., Smith, R. S., Straneo, F., Sun, S., Tarasov, L., Trusel, L. D., Van Breedam, J., van de Wal, R., van den Broeke, M., Winkelmann, R., Zekollari, H., Zhao, C., Zhang, T., and Zwinger, T.: Projected land ice contributions to twenty-first-century sea level rise, Nature, 593, 74–82, https://doi.org/10.1038/s41586-021-03302-y, 2021.
- Emanuelsson, B. D., Thomas, E. R., Tetzner, D. R., Humby, J. D., and Vladimirova, D. O.: Ice Core Chronologies from the Antarctic Peninsula: The Palmer, Jurassic, and Rendezvous Age-Scales, Geosciences, 12, 87, https://doi.org/10.3390/geosciences12020087, 2022.
 - Fretwell, P., Pritchard, H. D., Vaughan, D. G., Bamber, J. L., Barrand, N. E., Bell, R., Bianchi, C., Bingham, R. G., Blankenship, D. D., Casassa, G., Catania, G., Callens, D., Conway, H., Cook, A. J., Corr, H. F. J., Damaske, D., Damm, V., Ferraccioli, F., Forsberg, R., Fujita,



540

545



- S., Gim, Y., Gogineni, P., Griggs, J. A., Hindmarsh, R. C. A., Holmlund, P., Holt, J. W., Jacobel, R. W., Jenkins, A., Jokat, W., Jordan, T., King, E. C., Kohler, J., Krabill, W., Riger-Kusk, M., Langley, K. A., Leitchenkov, G., Leuschen, C., Luyendyk, B. P., Matsuoka, K.,
 Mouginot, J., Nitsche, F. O., Nogi, Y., Nost, O. A., Popov, S. V., Rignot, E., Rippin, D. M., Rivera, A., Roberts, J., Ross, N., Siegert, M. J.,
 Smith, A. M., Steinhage, D., Studinger, M., Sun, B., Tinto, B. K., Welch, B. C., Wilson, D., Young, D. A., Xiangbin, C., and Zirizzotti,
 A.: Bedmap2: improved ice bed, surface and thickness datasets for Antarctica, The Cryosphere, 7, 375–393, https://doi.org/10.5194/tc-7-375-2013, 2013.
- Fudge, T. J., Markle, B. R., Cuffey, K. M., Buizert, C., Taylor, K. C., Steig, E. J., Waddington, E. D., Conway, H., and Koutnik, M.: Variable relationship between accumulation and temperature in West Antarctica for the past 31,000 years, Geophysical Research Letters, 43, 3795–3803, https://doi.org/10.1002/2016GL068356, 2016.
 - Fujita, S., Matsuoka, T., Ishida, T., Matsuoka, K., and Mae, S.: A summary of the complex dielectric permittivity of ice in the megahertz range and its applications for radar sounding of polar ice sheets, Physics of Ice Core Records, pp. 185–212, 2000.
 - Fujita, S., Parrenin, F., Severi, M., Motoyama, H., and Wolff, E. W.: Volcanic synchronization of Dome Fuji and Dome C Antarctic deep ice cores over the past 216 kyr, Climate of the Past, 11, 1395–1416, https://doi.org/10.5194/cp-11-1395-2015, 2015.
 - Gardner, A. S., Moholdt, G., Scambos, T., Fahnstock, M., Ligtenberg, S., van den Broeke, M., and Nilsson, J.: Increased West Antarctic and unchanged East Antarctic ice discharge over the last 7 years, The Cryosphere, 12, 521–547, https://doi.org/10.5194/tc-12-521-2018, 2018.
 - Grieman, M. M., Hoffmann, H. M., Humby, J. D., Mulvaney, R., Nehrbass-Ahles, C., Rix, J., Thomas, E. R., Tuckwell, R., and Wolff, E. W.: Continuous flow analysis methods for sodium, magnesium and calcium detection in the Skytrain ice core, Journal of Glaciology, 68, 90–100, https://doi.org/10.1017/jog.2021.75, 2022.
 - Grieman, M. M., Nehrbass-Ahles, C., Hoffmann, H. M., Bauska, T. K., King, A. C. F., Mulvaney, R., Rhodes, R. H., Rowell, I. F., Thomas, E. R., and Wolff, E. W.: Abrupt Holocene ice loss due to thinning and ungrounding in the Weddell Sea Embayment, Nature Geoscience, 17, 227–232, https://doi.org/10.1038/s41561-024-01375-8, 2024.
- Hansen, P. C.: The L-curve and its use in the numerical treatment of inverse problems, in: InviteComputational Inverse Problems in Electrocardiology, WIT Press, 2000.
 - Hazzard, J. A. N. and Richards, F. D.: Antarctic Geothermal Heat Flow, Crustal Conductivity and Heat Production Inferred From Seismological Data, Geophysical Research Letters, 51, e2023GL106274, https://doi.org/10.1029/2023GL106274, 2024.
 - Hein, A. S., Marrero, S. M., Woodward, J., Dunning, S. A., Winter, K., Westoby, M. J., Freeman, S. P. H. T., Shanks, R. P., and Sugden, D. E.: Mid-Holocene pulse of thinning in the Weddell Sea sector of the West Antarctic ice sheet, Nature Communications, 7, 12511, https://doi.org/10.1038/ncomms12511, 2016.
 - Helm, V., Humbert, A., and Miller, H.: Elevation and elevation change of Greenland and Antarctica derived from CryoSat-2, The Cryosphere, 8, 1539–1559, https://doi.org/10.5194/tc-8-1539-2014, 2014.
- Hoffmann, H. M., Grieman, M. M., King, A. C. F., Epifanio, J. A., Martin, K., Vladimirova, D., Pryer, H. V., Doyle, E., Schmidt, A., Humby, J. D., Rowell, I. F., Nehrbass-Ahles, C., Thomas, E. R., Mulvaney, R., and Wolff, E. W.: The ST22 chronology for the Skytrain Ice Rise
 ice core Part 1: A stratigraphic chronology of the last 2000 years, Climate of the Past, 18, 1831–1847, https://doi.org/10.5194/cp-18-1831-2022, 2022.
 - Jones, R. S., Johnson, J. S., Lin, Y., Mackintosh, A. N., Sefton, J. P., Smith, J. A., Thomas, E. R., and Whitehouse, P. L.: Stability of the Antarctic Ice Sheet during the pre-industrial Holocene, Nature Reviews Earth & Environment, 3, 500–515, https://doi.org/10.1038/s43017-022-00309-5, 2022.





- Jordan, T. A., Martin, C., Ferraccioli, F., Matsuoka, K., Corr, H., Forsberg, R., Olesen, A., and Siegert, M.: Anomalously high geothermal flux near the South Pole, Scientific Reports, 8, 16785, https://doi.org/10.1038/s41598-018-35182-0, 2018.
 - Karlsson, N. B., Bingham, R. G., Rippin, D. M., Hindmarsh, R. C., Corr, H. F., and Vaughan, D. G.: Constraining past accumulation in the central Pine Island Glacier basin, West Antarctica, using radio-echo sounding, Journal of Glaciology, 60, 553–562, https://doi.org/10.3189/2014JoG13J180, 2014.
- 570 King, E. C.: The precision of radar-derived subglacial bed topography: a case study from Pine Island Glacier, Antarctica, Annals of Glaciology, 61, 154–161, https://doi.org/10.1017/aog.2020.33, 2020.
 - Kingslake, J., Scherer, R. P., Albrecht, T., Coenen, J., Powell, R. D., Reese, R., Stansell, N. D., Tulaczyk, S., Wearing, M. G., and Whitehouse, P. L.: Extensive retreat and re-advance of the West Antarctic Ice Sheet during the Holocene, Nature, 558, 430–434, https://doi.org/10.1038/s41586-018-0208-x, 2018.
- Koutnik, M. R., Fudge, T. J., Conway, H., Waddington, E. D., Neumann, T. A., Cuffey, K. M., Buizert, C., and Taylor, K. C.: Holocene accumulation and ice flow near the West Antarctic Ice Sheet Divide ice core site, Journal of Geophysical Research: Earth Surface, 121, 907–924, https://doi.org/10.1002/2015JF003668, 2016.
 - Lagarias, J. C., Reeds, J. A., Wright, M. H., and Wright, P. E.: Convergence Properties of the Nelder–Mead Simplex Method in Low Dimensions, SIAM Journal on Optimization, 9, 112–147, https://doi.org/10.1137/S1052623496303470, 1998.
- Larter, R. D., Anderson, J. B., Graham, A. G. C., Gohl, K., Hillenbrand, C.-D., Jakobsson, M., Johnson, J. S., Kuhn, G., Nitsche, F. O., Smith, J. A., Witus, A. E., Bentley, M. J., Dowdeswell, J. A., Ehrmann, W., Klages, J. P., Lindow, J., Cofaigh, C., and Spiegel, C.: Reconstruction of changes in the Amundsen Sea and Bellingshausen Sea sector of the West Antarctic Ice Sheet since the Last Glacial Maximum, Quaternary Science Reviews, 100, 55–86, https://doi.org/10.1016/j.quascirev.2013.10.016, 2014.
- Leysinger Vieli, G. J.-M. C., Martín, C., Hindmarsh, R. C. A., and Lüthi, M. P.: Basal freeze-on generates complex ice-sheet stratigraphy,

 Nature Communications, 9, 4669, https://doi.org/10.1038/s41467-018-07083-3, 2018.
 - Lilien, D. A., Steinhage, D., Taylor, D., Parrenin, F., Ritz, C., Mulvaney, R., Martín, C., Yan, J.-B., O'Neill, C., Frezzotti, M., Miller, H., Gogineni, P., Dahl-Jensen, D., and Eisen, O.: Brief communication: New radar constraints support presence of ice older than 1.5 Myr at Little Dome C, The Cryosphere, 15, 1881–1888, https://doi.org/10.5194/tc-15-1881-2021, 2021.
- Lliboutry, L. A.: A critical review of analytical approximate solutions for steady state velocities and temperatures in cold ice sheets., Z. Gletscherkde. Glazialgeol, 15, 135–148, 1979.
 - Lythe, M. B. and Vaughan, D. G.: BEDMAP: A new ice thickness and subglacial topographic model of Antarctica, Journal of Geophysical Research: Solid Earth, 106, 11 335–11 351, https://doi.org/10.1029/2000JB900449, 2001.
 - MacGregor, J. A., Boisvert, L. N., Medley, B., Petty, A. A., Harbeck, J. P., Bell, R. E., Blair, J. B., Blanchard-Wrigglesworth, E., Buckley, E. M., Christoffersen, M. S., Cochran, J. R., Csathó, B. M., De Marco, E. L., Dominguez, R. T., Fahnestock, M. A., Farrell, S. L., Gogineni, S. P., Greenbaum, J. S., Hansen, C. M., Hofton, M. A., Holt, J. W., Jezek, K. C., Koenig, L. S., Kurtz, N. T., Kwok, R., Larsen,
 - C. F., Leuschen, C. J., Locke, C. D., Manizade, S. S., Martin, S., Neumann, T. A., Nowicki, S. M., Paden, J. D., Richter-Menge, J. A., Rignot, E. J., Rodríguez-Morales, F., Siegfried, M. R., Smith, B. E., Sonntag, J. G., Studinger, M., Tinto, K. J., Truffer, M., Wagner, T. P., Woods, J. E., Young, D. A., and Yungel, J. K.: The Scientific Legacy of NASA's Operation IceBridge, Reviews of Geophysics, 59, e2020RG000712, https://doi.org/10.1029/2020RG000712, 2021.
- Martín, C. and Gudmundsson, G. H.: Effects of nonlinear rheology, temperature and anisotropy on the relationship between age and depth at ice divides, The Cryosphere, 6, 1221–1229, https://doi.org/10.5194/tc-6-1221-2012, 2012.

https://doi.org/10.1002/2017GL074954, 2017.



615

620



- Martín, C., Mulvaney, R., Gudmundsson, G. H., and Corr, H.: Inferring palaeo-accumulation records from ice-core data by an adjoint-based method: application to James Ross Island's ice core, Climate of the Past, 11, 547–557, https://doi.org/10.5194/cp-11-547-2015, 2015.
- Matsuoka, K., Skoglund, A., Roth, G., de Pomereu, J., Griffiths, H., Headland, R., Herried, B., Katsumata, K., Le Brocq, A., Licht, K., Morgan, F., Neff, P. D., Ritz, C., Scheinert, M., Tamura, T., Van de Putte, A., van den Broeke, M., von Deschwanden, A., Deschamps-Berger, C., Van Liefferinge, B., Tronstad, S., and Melvær, Y.: Quantarctica, an integrated mapping environment for Antarctica, the Southern Ocean, and sub-Antarctic islands, Environmental Modelling & Software, 140, 105 015, https://doi.org/10.1016/j.envsoft.2021.105015, 2021.
- Mercer, J. H.: West Antarctic ice sheet and CO2 greenhouse effect: a threat of disaster, Nature, 271, 321–325, https://doi.org/10.1038/271321a0, 1978.
 - Miles, B. W. J. and Bingham, R. G.: Progressive unanchoring of Antarctic ice shelves since 1973, Nature, 626, 785–791, https://doi.org/10.1038/s41586-024-07049-0, 2024.
 - Monnin, E., Steig, E. J., Siegenthaler, U., Kawamura, K., Schwander, J., Stauffer, B., Stocker, T. F., Morse, D. L., Barnola, J.-M., Bellier, B., Raynaud, D., and Fischer, H.: Evidence for substantial accumulation rate variability in Antarctica during the Holocene, through synchronization of CO2 in the Taylor Dome, Dome C and DML ice cores, Earth and Planetary Science Letters, 224, 45–54, https://doi.org/10.1016/j.epsl.2004.05.007, 2004.
 - Morlighem, M., Williams, C. N., Rignot, E., An, L., Arndt, J. E., Bamber, J. L., Catania, G., Chauché, N., Dowdeswell, J. A., Dorschel, B., Fenty, I., Hogan, K., Howat, I., Hubbard, A., Jakobsson, M., Jordan, T. M., Kjeldsen, K. K., Millan, R., Mayer, L., Mouginot, J., Noël, B. P. Y., O'Cofaigh, C., Palmer, S., Rysgaard, S., Seroussi, H., Siegert, M. J., Slabon, P., Straneo, F., van den Broeke, M. R., Weinrebe, W., Wood, M., and Zinglersen, K. B.: BedMachine v3: Complete Bed Topography and Ocean Bathymetry Mapping of Greenland From Multibeam Echo Sounding Combined With Mass Conservation, Geophysical Research Letters, 44, 11,051–11,061,
 - Mulvaney, R., Wolff, E. W., Grieman, M. M., Hoffmann, H. H., Humby, J. D., Nehrbass-Ahles, C., Rhodes, R. H., Rowell, I. F., Parrenin, F., Schmidely, L., Fischer, H., Stocker, T. F., Christl, M., Muscheler, R., Landais, A., and Prié, F.: The ST22 chronology for the Skytrain Ice Rise ice core Part 2: An age model to the last interglacial and disturbed deep stratigraphy, Climate of the Past, 19, 851–864, https://doi.org/10.5194/cp-19-851-2023, 2023.
 - Mutter, E. L. and Holschuh, N.: Advancing interpretation of incoherent scattering in ice penetrating radar data used for ice core site selection, EGUsphere, pp. 1–27, https://doi.org/10.5194/egusphere-2024-2450, 2024.
- Narcisi, B., Robert Petit, J., and Tiepolo, M.: A volcanic marker (92 ka) for dating deep east Antarctic ice cores, Quaternary Science Reviews, 25, 2682–2687, https://doi.org/10.1016/j.quascirev.2006.07.009, 2006.
 - Neumann, T. A., Conway, H., Price, S. F., Waddington, E. D., Catania, G. A., and Morse, D. L.: Holocene accumulation and ice sheet dynamics in central West Antarctica, Journal of Geophysical Research: Earth Surface, 113, https://doi.org/10.1029/2007JF000764, 2008.
 - Nilsson, J., Gardner, A. S., and Paolo, F. S.: Elevation change of the Antarctic Ice Sheet: 1985 to 2020, Earth System Science Data, 14, 3573–3598, https://doi.org/10.5194/essd-14-3573-2022, 2022.
- Nye, J. F.: Correction Factor for Accumulation Measured by the Thickness of the Annual Layers in an Ice Sheet, Journal of Glaciology, 4, 785–788, https://doi.org/10.3189/S0022143000028367, 1963.
 - Otosaka, I. N., Shepherd, A., Ivins, E. R., Schlegel, N.-J., Amory, C., van den Broeke, M. R., Horwath, M., Joughin, I., King, M. D., Krinner, G., Nowicki, S., Payne, A. J., Rignot, E., Scambos, T., Simon, K. M., Smith, B. E., Sørensen, L. S., Velicogna, I., Whitehouse, P. L., A, G., Agosta, C., Ahlstrøm, A. P., Blazquez, A., Colgan, W., Engdahl, M. E., Fettweis, X., Forsberg, R., Gallée, H., Gardner, A., Gilbert, L.,



650



- Gourmelen, N., Groh, A., Gunter, B. C., Harig, C., Helm, V., Khan, S. A., Kittel, C., Konrad, H., Langen, P. L., Lecavalier, B. S., Liang, C.-C., Loomis, B. D., McMillan, M., Melini, D., Mernild, S. H., Mottram, R., Mouginot, J., Nilsson, J., Noël, B., Pattle, M. E., Peltier, W. R., Pie, N., Roca, M., Sasgen, I., Save, H. V., Seo, K.-W., Scheuchl, B., Schrama, E. J. O., Schröder, L., Simonsen, S. B., Slater, T., Spada, G., Sutterley, T. C., Vishwakarma, B. D., van Wessem, J. M., Wiese, D., van der Wal, W., and Wouters, B.: Mass balance of the Greenland and Antarctic ice sheets from 1992 to 2020, Earth System Science Data, 15, 1597–1616, https://doi.org/10.5194/essd-15-1597-2023, 2023.
- Palmer, A. S., van Ommen, T. D., Curran, M. A. J., Morgan, V., Souney, J. M., and Mayewski, P. A.: High-precision dating of volcanic events (A.D. 1301–1995) using ice cores from Law Dome, Antarctica, Journal of Geophysical Research: Atmospheres, 106, 28 089–28 095, https://doi.org/10.1029/2001JD000330, 2001.
 - Parrenin, F., Dreyfus, G., Durand, G., Fujita, S., Gagliardini, O., Gillet, F., Jouzel, J., Kawamura, K., Lhomme, N., Masson-Delmotte, V., Ritz, C., Schwander, J., Shoji, H., Uemura, R., Watanabe, O., and Yoshida, N.: 1-D-ice flow modelling at EPICA Dome C and Dome Fuji, East Antarctica, Climate of the Past, 3, 243–259, https://doi.org/10.5194/cp-3-243-2007, 2007.
 - Pattyn, F. and Morlighem, M.: The uncertain future of the Antarctic Ice Sheet, Science, 367, 1331–1335, https://doi.org/10.1126/science.aaz5487, 2020.
 - Pritchard, H. D., Arthern, R. J., Vaughan, D. G., and Edwards, L. A.: Extensive dynamic thinning on the margins of the Greenland and Antarctic ice sheets, Nature, 461, 971–975, https://doi.org/10.1038/nature08471, 2009.
- Pritchard, H. D., Fretwell, P. T., Fremand, A. C., Bodart, J. A., Kirkham, J. D., Aitken, A., Bamber, J., Bell, R., Bianchi, C., Bingham, R. G., Blankenship, D. D., Casassa, G., Christianson, K., Conway, H., Corr, H. F. J., Cui, X., Damaske, D., Damm, V., Dorschel, B., Drews, R., Eagles, G., Eisen, O., Eisermann, H., Ferraccioli, F., Field, E., Forsberg, R., Franke, S., Goel, V., Gogineni, S. P., Greenbaum, J., Hills, B., Hindmarsh, R. C. A., Hoffman, A. O., Holschuh, N., Holt, J. W., Humbert, A., Jacobel, R. W., Jansen, D., Jenkins, A., Jokat, W., Jong, L., Jordan, T. A., King, E. C., Kohler, J., Krabill, W., Maton, J., Gillespie, M. K., Langley, K., Lee, J., Leitchenkov, G.,
- Leuschen, C., Luyendyk, B., MacGregor, J. A., MacKie, E., Moholdt, G., Matsuoka, K., Morlighem, M., Mouginot, J., Nitsche, F. O., Nost, O. A., Paden, J., Pattyn, F., Popov, S., Rignot, E., Rippin, D. M., Rivera, A., Roberts, J. L., Ross, N., Ruppel, A., Schroeder, D. M., Siegert, M. J., Smith, A. M., Steinhage, D., Studinger, M., Sun, B., Tabacco, I., Tinto, K. J., Urbini, S., Vaughan, D. G., Wilson, D. S., Young, D. A., and Zirizzotti, A.: Bedmap3 updated ice bed, surface and thickness gridded datasets for Antarctica, Scientific Data, 12, 414, https://doi.org/10.1038/s41597-025-04672-y, 2025.
- 665 Raynaud, D. and Lebel, B.: Total gas content and surface elevation of polar ice sheets, Nature, 281, 289–291, https://doi.org/10.1038/281289a0, 1979.
 - Rodriguez-Morales, F., Gogineni, S., Leuschen, C. J., Paden, J. D., Li, J., Lewis, C. C., Panzer, B., Gomez-Garcia Alvestegui, D., Patel, A., Byers, K., Crowe, R., Player, K., Hale, R. D., Arnold, E. J., Smith, L., Gifford, C. M., Braaten, D., and Panton, C.: Advanced Multifrequency Radar Instrumentation for Polar Research, IEEE Transactions on Geoscience and Remote Sensing, 52, 2824–2842, https://doi.org/10.1109/TGRS.2013.2266415, 2014.
 - Ross, N., Bingham, R. G., Corr, H. F. J., Ferraccioli, F., Jordan, T. A., Le Brocq, A., Rippin, D. M., Young, D., Blankenship, D. D., and Siegert, M. J.: Steep reverse bed slope at the grounding line of the Weddell Sea sector in West Antarctica, Nature Geoscience, 5, 393–396, https://doi.org/10.1038/ngeo1468, 2012.
- Rowell, I., Martin, C., Mulvaney, R., Pryer, H., Tetzner, D., Doyle, E., Talasila, H. M., Li, J., and Wolff, E.: An age scale for new climate records from Sherman Island, West Antarctica, Climate of the Past, 19, 1699–1714, https://doi.org/10.5194/cp-19-1699-2023, 2023.
 - Scambos, T. A., Bell, R. E., Alley, R. B., Anandakrishnan, S., Bromwich, D. H., Brunt, K., Christianson, K., Creyts, T., Das, S. B., DeConto, R., Dutrieux, P., Fricker, H. A., Holland, D., MacGregor, J., Medley, B., Nicolas, J. P., Pollard, D., Siegfried, M. R.,





- Smith, A. M., Steig, E. J., Trusel, L. D., Vaughan, D. G., and Yager, P. L.: How much, how fast?: A science review and outlook for research on the instability of Antarctica's Thwaites Glacier in the 21st century, Global and Planetary Change, 153, 16–34, https://doi.org/10.1016/j.gloplacha.2017.04.008, 2017.
 - Shepherd, A., Gilbert, L., Muir, A. S., Konrad, H., McMillan, M., Slater, T., Briggs, K. H., Sundal, A. V., Hogg, A. E., and Engdahl, M. E.: Trends in Antarctic Ice Sheet Elevation and Mass, Geophysical Research Letters, 46, 8174–8183, https://doi.org/10.1029/2019GL082182, 2019.
- Siegert, M., Ross, N., Corr, H., Kingslake, J., and Hindmarsh, R.: Late Holocene ice-flow reconfiguration in the Weddell Sea sector of West Antarctica, Quaternary Science Reviews, 78, 98–107, https://doi.org/10.1016/j.quascirev.2013.08.003, 2013.
 - Siegert, M. J.: On the origin, nature and uses of Antarctic ice-sheet radio-echo layering, Progress in Physical Geography: Earth and Environment, 23, 159–179, https://doi.org/10.1177/030913339902300201, 1999.
 - Siegert, M. J. and Payne, A. J.: Past rates of accumulation in central West Antarctica, Geophysical Research Letters, 31, https://doi.org/10.1029/2004GL020290, 2004.
- Sigl, M., Fudge, T. J., Winstrup, M., Cole-Dai, J., Ferris, D., McConnell, J. R., Taylor, K. C., Welten, K. C., Woodruff, T. E., Adolphi, F., Bisiaux, M., Brook, E. J., Buizert, C., Caffee, M. W., Dunbar, N. W., Edwards, R., Geng, L., Iverson, N., Koffman, B., Layman, L., Maselli, O. J., McGwire, K., Muscheler, R., Nishiizumi, K., Pasteris, D. R., Rhodes, R. H., and Sowers, T. A.: The WAIS Divide deep ice core WD2014 chronology Part 2: Annual-layer counting (0–31 ka BP), Climate of the Past, 12, 769–786, https://doi.org/10.5194/cp-12-769-2016, 2016.
- 695 Staniforth, A. and Côté, J.: Semi-Lagrangian Integration Schemes for Atmospheric Models—A Review, 1991.
 - Sutter, J., Fischer, H., and Eisen, O.: Investigating the internal structure of the Antarctic ice sheet: the utility of isochrones for spatiotemporal ice-sheet model calibration, The Cryosphere, 15, 3839–3860, https://doi.org/10.5194/tc-15-3839-2021, 2021.
 - Thomas, E. R. and Bracegirdle, T. J.: Precipitation pathways for five new ice core sites in Ellsworth Land, West Antarctica, Climate Dynamics, 44, 2067–2078, https://doi.org/10.1007/s00382-014-2213-6, 2014.
- Thomas, E. R., Bracegirdle, T. J., Turner, J., and Wolff, E. W.: A 308 year record of climate variability in West Antarctica, Geophysical Research Letters, 40, 5492–5496, https://doi.org/10.1002/2013GL057782, 2013.
 - Thomas, E. R., Hosking, J. S., Tuckwell, R. R., Warren, R. A., and Ludlow, E. C.: Twentieth century increase in snowfall in coastal West Antarctica, Geophysical Research Letters, 42, 9387–9393, https://doi.org/10.1002/2015GL065750, 2015.
- Thomas, E. R., van Wessem, J. M., Roberts, J., Isaksson, E., Schlosser, E., Fudge, T. J., Vallelonga, P., Medley, B., Lenaerts, J., Bertler, N., van den Broeke, M. R., Dixon, D. A., Frezzotti, M., Stenni, B., Curran, M., and Ekaykin, A. A.: Regional Antarctic snow accumulation over the past 1000 years, Climate of the Past, 13, 1491–1513, https://doi.org/10.5194/cp-13-1491-2017, 2017.
 - Thomas, R. H. and Bentley, C. R.: A Model for Holocene Retreat of the West Antarctic Ice Sheet, Quaternary Research, 10, 150–170, https://doi.org/10.1016/0033-5894(78)90098-4, 1978.
- Turner, J., Orr, A., Gudmundsson, G. H., Jenkins, A., Bingham, R. G., Hillenbrand, C.-D., and Bracegirdle, T. J.: Atmosphere-ocean-ice inter-actions in the Amundsen Sea Embayment, West Antarctica, Reviews of Geophysics, 55, 235–276, https://doi.org/10.1002/2016RG000532, 2017.
 - Vaughan, D. G., Corr, H. F. J., Ferraccioli, F., Frearson, N., O'Hare, A., Mach, D., Holt, J. W., Blankenship, D. D., Morse, D. L., and Young, D. A.: New boundary conditions for the West Antarctic ice sheet: Subglacial topography beneath Pine Island Glacier, Geophysical Research Letters, 33, https://doi.org/10.1029/2005GL025588, 2006.





- 715 Weertman, J.: Stability of the Junction of an Ice Sheet and an Ice Shelf, Journal of Glaciology, 13, 3–11, https://doi.org/10.3189/S0022143000023327, 1974.
 - Wolff, E. W., Mulvaney, R., Grieman, M. M., Hoffmann, H. M., Humby, J., Nehrbass-Ahles, C., Rhodes, R. H., Rowell, I. F., Sime, L. C., Fischer, H., Stocker, T. F., Landais, A., Parrenin, F., Steig, E. J., Dütsch, M., and Golledge, N. R.: The Ronne Ice Shelf survived the last interglacial, Nature, pp. 1–5, https://doi.org/10.1038/s41586-024-08394-w, 2025.
- Wolovick, M., Humbert, A., Kleiner, T., and Rückamp, M.: Regularization and L-curves in ice sheet inverse models: a case study in the Filchner–Ronne catchment, The Cryosphere, 17, 5027–5060, https://doi.org/10.5194/tc-17-5027-2023, 2023.
 - Wouters, B., Martin-Español, A., Helm, V., Flament, T., van Wessem, J. M., Ligtenberg, S. R. M., van den Broeke, M. R., and Bamber, J. L.: Dynamic thinning of glaciers on the Southern Antarctic Peninsula, Science, 348, 899–903, https://doi.org/10.1126/science.aaa5727, 2015.
- Zwally, H. J., Giovinetto, M. B., Beckley, M. A., and Saba, J. L.: Antarctic and Greenland Drainage Systems, GSFC Cryospheric Sciences
 Laboratory, 2012.